

**Loss of Cln5 leads to altered Gad1 expression and deficits in interneuron development in mice**

Journal:	<i>Human Molecular Genetics</i>
Manuscript ID	HMG-2019-D-00066.R1
Manuscript Type:	2 General Article - UK Office
Date Submitted by the Author:	n/a
Complete List of Authors:	<p>Singh, Yajuvinder; University of Eastern Finland, A. I. Virtanen Institute for Molecular Sciences</p> <p>Leinonen, Henri; University of Eastern Finland, A. I. Virtanen Institute for Molecular Sciences; University of California Irvine School of Medicine, Department of Ophthalmology</p> <p>Fazaludeen, Feroze; University of Eastern Finland, A. I. Virtanen Institute for Molecular Sciences</p> <p>Jaronen, Merja; University of Eastern Finland, A. I. Virtanen Institute for Molecular Sciences</p> <p>Guest, Debbie; Animal Health Trust, Animal Health Trust</p> <p>Buckley, Noel; University of Oxford, Department of Psychiatry</p> <p>Byts, Nadiya; University of Oulu, Oulu Centre for Cell Matrix Research, Biocenter Oulu and Faculty of Biochemistry and Molecular Medicine</p> <p>Oksa, Petra; University of Eastern Finland, A. I. Virtanen Institute for Molecular Sciences</p> <p>Jalkanen, Kari; University of Eastern Finland, A. I. Virtanen Institute for Molecular Sciences</p> <p>Iqbal, Imran; University of Eastern Finland, A. I. Virtanen Institute for Molecular Sciences</p> <p>Huuskonen, Mikko; University of Eastern Finland, A. I. Virtanen Institute for Molecular Sciences</p> <p>Savchenko, Ekaterina; University of Eastern Finland, A. I. Virtanen Institute for Molecular Sciences</p> <p>Keksa-Goldsteine, Velta; University of Eastern Finland, A. I. Virtanen Institute for Molecular Sciences</p> <p>Chew, Sweelin; University of Eastern Finland, A. I. Virtanen Institute for Molecular Sciences</p> <p>Myllyharju, Johanna; University of Oulu, Oulu Centre for Cell Matrix Research, Biocenter Oulu and Faculty of Biochemistry and Molecular Medicine</p> <p>Tanila, Heikki; University of Eastern Finland, A. I. Virtanen Institute for Molecular Sciences</p> <p>Ooi, Lezanne; University of Wollongong, Illawarra Health and Medical Research Institute, School of Biological Sciences</p> <p>Koistinaho, Jari; University of Eastern Finland, A. I. Virtanen Institute for Molecular Sciences</p> <p>Kanninen, Katja; University of Eastern Finland, A. I. Virtanen Institute for Molecular Sciences</p> <p>Malm, Tarja; University of Eastern Finland, A. I. Virtanen Institute for</p>

1  
2  
3  
4  
5  
6  
7  
8  
9  
10  
11  
12  
13  
14  
15  
16  
17  
18  
19  
20  
21  
22  
23  
24  
25  
26  
27  
28  
29  
30  
31  
32  
33  
34  
35  
36  
37  
38  
39  
40  
41  
42  
43  
44  
45  
46  
47  
48  
49  
50  
51  
52  
53  
54  
55  
56  
57  
58  
59  
60

	Molecular Sciences
Key Words:	Embryonic development, Neurodegenerative disease, Neuronal Ceroid Lipofuscinosis, Lysosomal storage disease, Pediatrics

SCHOLARONE™  
Manuscripts

## REVIEWERS' COMMENTS

We have carried out a large number of new experiments to answer the reviewer comments, as outlined below. A new author, Dr Sweelin Chew, has therefore been added to the author list.

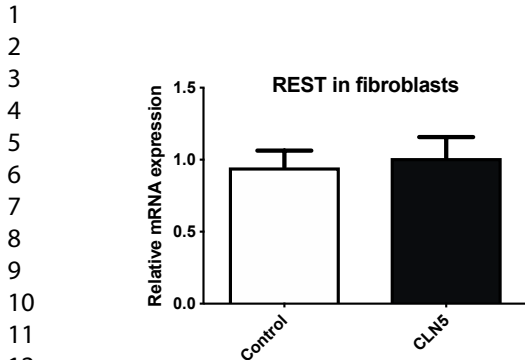
### Reviewer: 1

**How the lack of a lysosomal protein affects development and more specifically interneuron development remains open. It remains unclear, how CLN5 regulates the levels of REST.**

*This is a good point. Although the direct mechanisms how CLN5 regulates the levels of REST is beyond the scope of this study, there are a number of studies providing evidence that conditions related to cell stress increase the levels of REST (1, 2). These include oxidative stress (1), inflammation (3), ischaemia (4) and epileptic seizure (5). Importantly, oxidative stress and inflammation are implicated in several NCL forms (6-8) and a well-established feature of the pathology in the CLN5-KO mice used in this study. The increase of REST is believed to protect neurons from oxidative stress and consequently, REST downregulation has been shown to lead to neurodegeneration (1). Loss of Cln5 alters proliferation, differentiation and apoptotic cell death. We propose that the loss of the lysosomal protein Cln5, increases inflammation and oxidative stress, leading to an upregulation of REST and a consequent downregulation of genes required for GABAergic differentiation, including Gad67 and Ptfla. Importantly, we show for the first time that this may occur through direct interaction of REST with Gad67. Ptfla is expressed in precursors to GABAergic neurons and is required for both early and late interneuron development (9). Consequently, misspecification of neurons in Ptfla-null mice results in a complete loss of inhibitory GABAergic neurons. This pathway is mediated by Lhx5 and Pax2, both of which were also identified as REST target genes (manuscript table S1). Together these findings suggest that REST regulates a panel of genes necessary for interneuron development. We have now amended the discussion accordingly.*

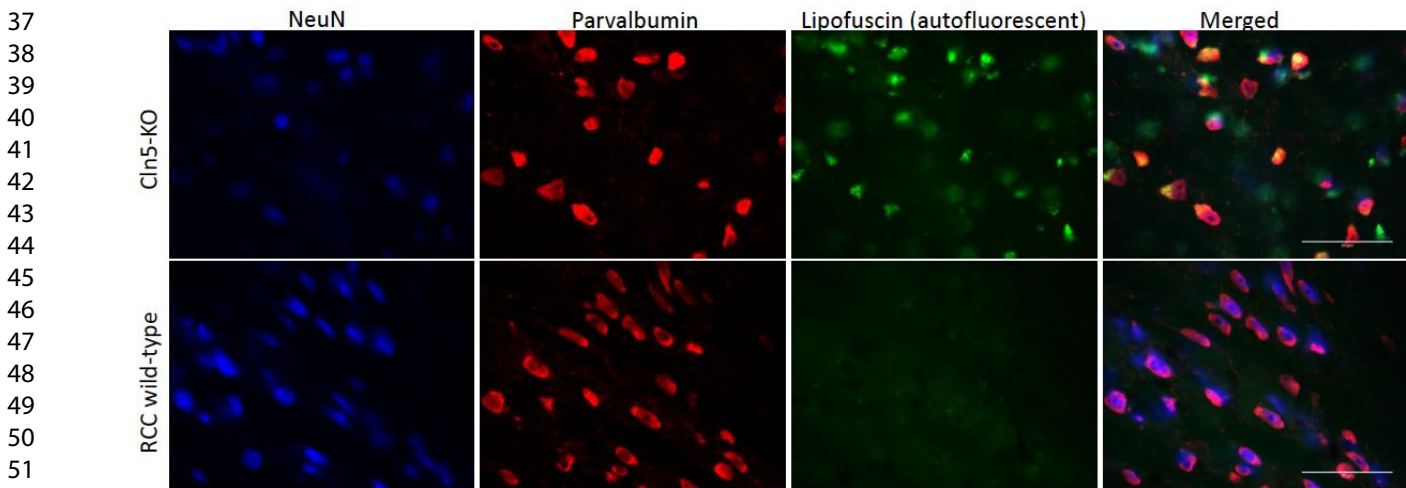
**How the findings are related to the human disease is also unclear. Is the contribution of the developmental delay indeed an important component of the human disease? This question is relevant in regard to possible future therapeutic approaches and the time point to start such therapies, like gene therapy.**

*As the reviewer is aware, the NCLs affect primarily children, and thus it is very difficult to access material for study from the patients. In an attempt to address whether the changes we observed in the CLN5-KO mouse model are represented in humans, we have obtained fibroblasts from healthy controls and two children suffering from Cln5 disease. These precious samples were probed for REST expression by qPCR, but no differences were observed (data shown below). This did not come as a surprise given that fibroblasts are very different from CNS cells, and thus cannot be directly compared to our observations in CLN5-KO mice. We do however think, based on our data, that a developmental delay is a component of CLN5 deficiency and feel that this initial finding is very important, and deserves to be considered in future studies of also other NCL forms. Further studies to fully delineate the contribution of developmental delay to this disease are beyond the scope of the current study, but clearly required.*

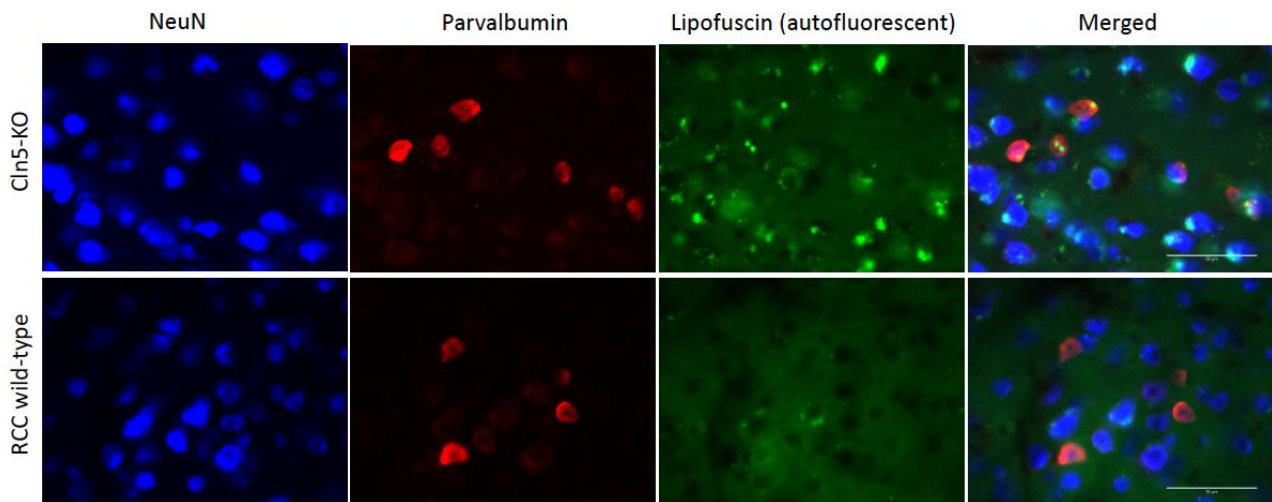


15 **The typical hallmark of NCLs is the accumulation of neuronal ceroid lipofuscin, and typically**  
16 **hydrophobic proteins proteins like saposins and subunit C of the mitochondrial ATPase**  
17 **(SCMAS) accumulate in lysosomes. Lysosome-size is strikingly increased. The authors should**  
18 **include experiments in which they show, if CLN5 KO mice, maybe in neuronal subpopulations**  
19 **(e.g. PV-positive), show already signs of lysosomal storage, e.g. by LAMP-**  
20 **immunohistochemistry, histology for autofluorescence, SCMAS-immunohistochemistry or**  
21 **even electron microscopy at early developmental stages, and also in comparison to adult mice:**  
22 **are PV-positive cells more heavily affected compared to others?**  
23  
24

25 *As suggested by the reviewer, we have carried out a double immunohistochemical staining for the*  
26 *neuronal nuclear antigen Neu and parvalbumin (PV) in CLN5-KO mouse brain sections. While the*  
27 *embryonic mouse brains show no autofluorescence, coronal brain sections of adult CLN5-KO mice*  
28 *displayed autofluorescence for lipofuscin in PV-positive neurons in the cortex, hippocampus and in*  
29 *the thalamus. Conversely, little autofluorescence was detected in adult wildtype mice (example*  
30 *images shown below). These results indicate that the PV-positive subpopulation of cells shows some*  
31 *evidence of lysosomal storage in adult mice. The fact that both PV-positive cells and PV-negative*  
32 *neuronal cells appear to be equally affected suggests that autofluorescence is not specific only for*  
33 *the PV-positive neurons.*  
34  
35



52 *Thalamus, Scale bar 100 um.*  
53  
54  
55  
56  
57  
58  
59  
60



Cortex, Scale bar 50  $\mu$ m.

**Previous papers suggested a major role of CLN5 in myelination. Could the changes observed in adult mice, including the behavioral data, related to altered myelination? This possibility should be at least discussed.**

*Indeed, earlier studies in the CLN5-KO mice have revealed a generalized early myelinisation defect, which did not progress between the ages of 1 and 3 months (10). In general, it is quite difficult to assess the contribution of hypomyelination to behavior, since in all models there are additional neurodevelopmental changes or other pathology such as neuroinflammation in induced hypomyelination models. In terms of the current study, it is possible that the demyelination contributes to the observed impairment in the Rotarod test, that draws on fast communication between the cerebellum and spinal cord via long myelinated axons. This has now been discussed in the manuscript.*

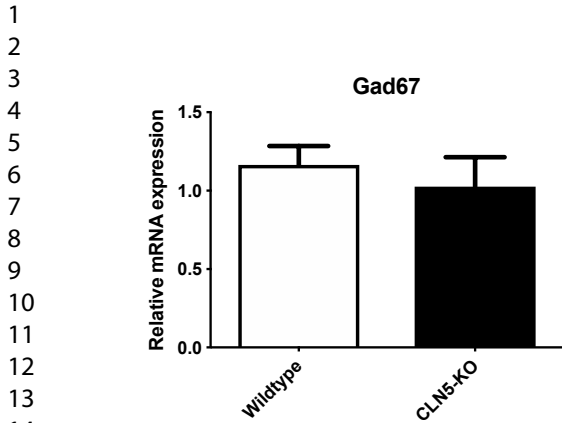
**The authors mention a ChIP microarray experiment that led to the conclusion, that REST regulates GABAergic development. If possible, these data should be included in the supplement.**

*Selected highly enriched genes in ChIP microarrays in NS5 cells are now shown in Table 1. All the data has been added in the supplementary data section of the manuscript.*

**ChIP-qPCR from NS5-cells and hippocampal samples confirmed the regulation of *Gag67* and *Ptf1a* by REST. The authors should include qPCR experiments (from hippocampal samples) to measure global expression changes of those genes in total RNA samples (not ChIP).**

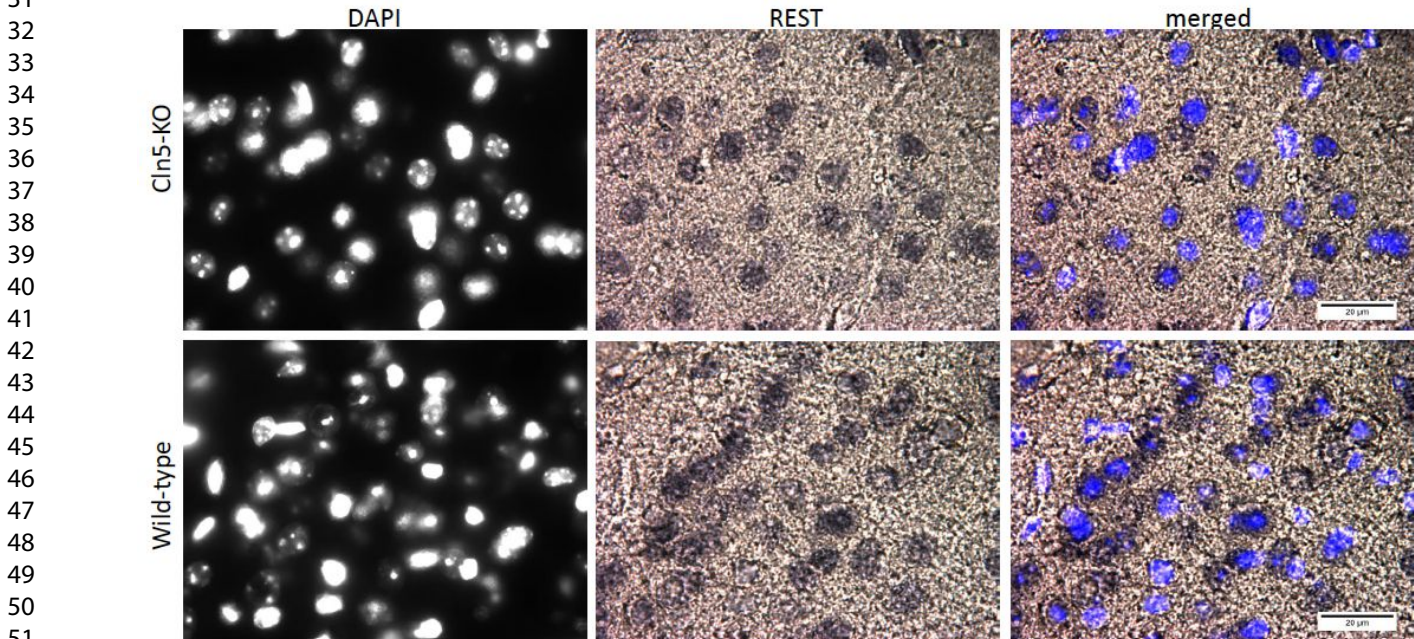
*As suggested by the reviewer, we have now carried out mRNA expression analyses in the hippocampi of 6-month old wildtype and CLN5-KO mice by qPCR. Global expression of *Gad67* was not altered in the CLN5-KO hippocampi. This is now mentioned in the results section of the manuscript. The levels of *Ptf1a* were too low for detection by qPCR (data not shown).*



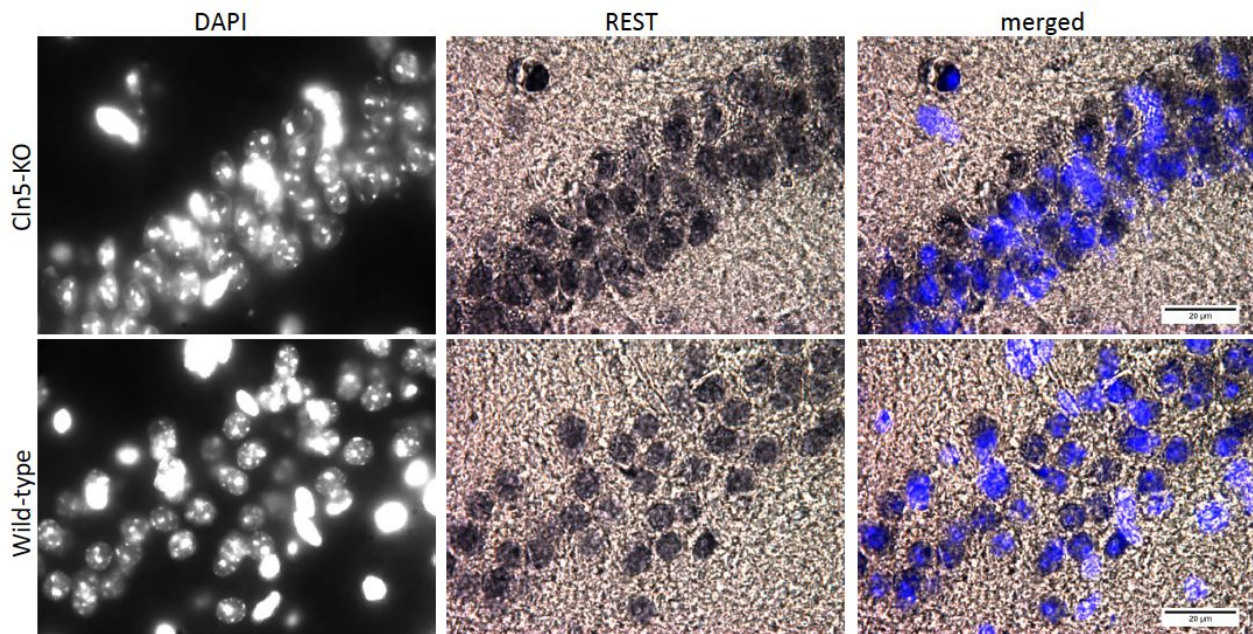


17 I'm wondering if, both in E14.5 animals and adult CLN5 KO animals, a redistribution of REST  
18 can be observed... antibodies for immunohistochemistry have been described  
19 (e.g. <https://www.ncbi.nlm.nih.gov/pubmed/24670762>) . This should be tested experimentally.

20  
21  
22 *As suggested by the reviewer, we have carried out immunohistochemical stainings for REST in the*  
23 *CLN5-KO mice. Brains sections were co-labelled for REST and DAPI, a DNA counterstain. Ni-DAB*  
24 *development was used to reduce the effect of autofluorescence on image quality. Images acquired*  
25 *under 60x magnification with 2x zoom reveal that the majority of REST appears to be located within*  
26 *the nuclei in the cortex as well as hippocampus of CLN5-KO mice. No visible difference in REST*  
27 *redistribution between wildtype and CLN5-KO was observed (images below). This suggests that*  
28 *REST re-distribution is not behind the observed effects. This has now also been mentioned in the*  
29 *manuscript.*



52 *Cortex, scale bar 20 μm.*



Hippocampus, scale bar 20  $\mu$ m.

Minor:

**1.) Introduction (lane 19):** It is meanwhile well accepted, that CLN5 is a soluble lysosomal glycoprotein (not “speculated”).

*The term ‘speculated’ has now been changed to “well accepted”.*

**2.) The discussion should be shortened significantly.**

*As suggested by the reviewer, we have attempted to shorten the discussion section. However, several of the points raised by the reviewers have required lengthening the discussion by including more explanation, making it very difficult to reduce the overall length of this section.*

## **Reviewer: 2**

**The authors seem to make on finding (that in and of itself is interesting) but then they don't link that finding directly to the next step in their story. Instead these take a few steps forward in the logic so that key pieces of the story seems to be missing. In some cases this can resolved with more explanation of the data but in others it may require additional experiments to fill in the gaps.**

*As requested by all reviewers, we have now carried out numerous extra experiments to address these comments, fulfill gaps and to make the story more logical. For instance, the order of figures has been changed and one previous figure was split into two to make the links between steps stronger. We have also attempted to further explain the data in the updated manuscript.*



1  
2  
3 **1) The authors state that there are 14 NCLs - although the numbers run 1-14 in the gene names,**  
4 **there is no CLN9 (so only 13 NCLs).**  
5

6 *This has now been corrected in the introduction section.*  
7  
8  
9

10 **2) The authors state that there are no changes in Nestin+ cells yet there is an increase in Pax6+**  
11 **cells in the ventricular zone. Shouldn't all Nestin+ radial progenitors also be Pax6+? Therefore,**  
12 **its unclear how these numbers differ?**  
13

14 *This is a good point and we thank the reviewer for bringing this up so that we can clarify the issue.*  
15 *Indeed, in the developing brain virtually all Pax6+ cells are also positive to nestin, as shown by Götz*  
16 *et al (1998, Neuron). However, the authors nicely show that there is a significant proportion of cells*  
17 *that are nestin positive but Pax6 negative. This pax6 negative but nestin positive population could*  
18 *overcome the observed difference in the extent of Pax6 positive and nestin positive cell populations.*  
19 *We have now modified the discussion part accordingly.*  
20  
21  
22  
23

24 **3) The authors mention that there are increased Pax6+ cells but decreased TuJ1+ cells during**  
25 **early corticogenesis. There could be many causes for this. Is the radial scaffold intact (the**  
26 **author have supplemental data that the Nestin+ numbers don't change but show no Nestin**  
27 **images to be able to determine if the scaffold itself is ok. Is the increase in Pax6+ cells because**  
28 **there are changes in the length/dynamics of the cell cycle -- ie., the cells are remaining as apical**  
29 **progenitors longer and not exiting the cell cycle. The authors use the Pax6+ increase to make**  
30 **a statement that proliferation of cells in the dorsal VZ is increased, but they don't actually**  
31 **directly look at this. The authors did Ph3 counts in the GE but could do the same counts in the**  
32 **dorsal ventricular zone to understand more about these Pax6+ cells and the proliferation in this**  
33 **compartment. Are the apical progenitors ever transitioning to become basal progenitors (are**  
34 **they moving away from the ventricular zone to SVZ or becoming Tbr2+ progenitors)?**  
35  
36  
37

38 *This is an important point and indeed, an increase in the PAX-6 staining in the dorsal telencephalon*  
39 *can be a result of several factors such as changes in proliferation, scaffolding, cell death rate,*  
40 *changes in cell fate choice or any combination of these factors. As kindly suggested by the reviewer*  
41 *to exclude the possibility that increase in PAX-6 immunoreactivity in CLN5-KO embryos may have*  
42 *been due to abnormal RG scaffolds, we examined RG scaffolding with nestin staining at E14.5.*  
43 *However, for the majority of the sections the staining did not show any gross changes in RG*  
44 *morphology (Figure S1A,B) suggesting that radial glial fibers are likely functionally normal in*  
45 *CLN5-KO embryos.*  
46  
47

48 *As suggested by the reviewers, we also analyzed the proliferative activity in the dorsal telencephalon*  
49 *with Ph3 counts. We observed a strong trend of an increase in the Ph3 counts in the dorsal*  
50 *telencephalon of E14.5 (intermediate and caudal sections) Fig. 2D-F). Thus, although we failed to*  
51 *provide double stainings for PAX6 and Ph3, our data suggests that PAX-6 increase was most likely*  
52 *due to an increase in the proliferative activity of the progenitor cells in the CLN5-KO embryos. We*  
53 *have now amended the discussion accordingly.*  
54  
55

56 **3) the authors perform TUNEL staining and counting in the cortical plate and GE. Although**  
57 **they don't say it directly, you are led to believe that the increases TUNEL in the cortical plate**  
58 **is correlated with the decreased interneurons being generated in the MGE. However the**  
59 **timepoints analyzed would match this story -- at E14.5 the migrating MGE derived**  
60



interneurons would not have reached the dorsal cortex. And when they come in, they enter in a dorsal and ventral stream -- yet the TUNEL + cells are throughout the cortical wall. So what are the cells that are dying? In the first set of figures, TuJ1 neurons are decreased at E14.5 but catch up by birth -- so how do you have decreased neurons at the peak of corticogenesis, increased cell death but things normalize by birth?

*The migration of interneurons from the ganglionic eminences (GEs) towards the dorsal pallium can roughly be divided into three waves (Reviewed by Marin et al. 2001). Early wave of migration begins around E11.5 where interneurons originating from medial ganglionic eminence (MGE) and anterior entopeduncular area (AEP) follow a superficial route to the developing striatum and invade marginal zone (MZ) and subplate (SP) in the cortex. Around E12.5-E14.5, when the MGE is the principal source of interneurons, they migrate tangentially into the cortex. These MGE derived interneurons either follow a deep or superficial migratory route and populate the sub ventricular zone (SVZ)/lower intermediate zone (IZ) and SP from where they eventually move on to the cortical plate. It is around E14.5-E1.6 that the late stage of interneuron migration occurs from both lateral ganglionic eminence (LGE) and MGE. As discussed above, although tangential migration is not fully complete by E14.5 but the cortex wall may well have a small number of interneuronal populations by this time point (mainly located in SVZ/IZ) therefore, the possibility of no involvement of interneuronal apoptosis in the cortex cannot be ruled out totally at E14.5. Developing brain has a high rate of apoptosis that involves cells from both the proliferative and post mitotic neuronal compartments (Burek et al. 1999; Rabinowicz et al. 1999; Rakic et al. 2001). Our studies indicate that at E14.5 Cln5-KO embryos have an abnormal rate of cell death when compared to the WT embryos, which can be seen throughout the entire telencephalic wall in the dorsal pallidum. Therefore, it is likely that in Cln5-KO embryos there is a high rate of apoptosis both in the precursor populations and in the post mitotic neurons. In support of the latter, we see that Tuj-1 positive staining is already decreased in the Cln5-KO mice, suggesting that neuronal apoptosis could be an important factor behind the loss of these neurons.*

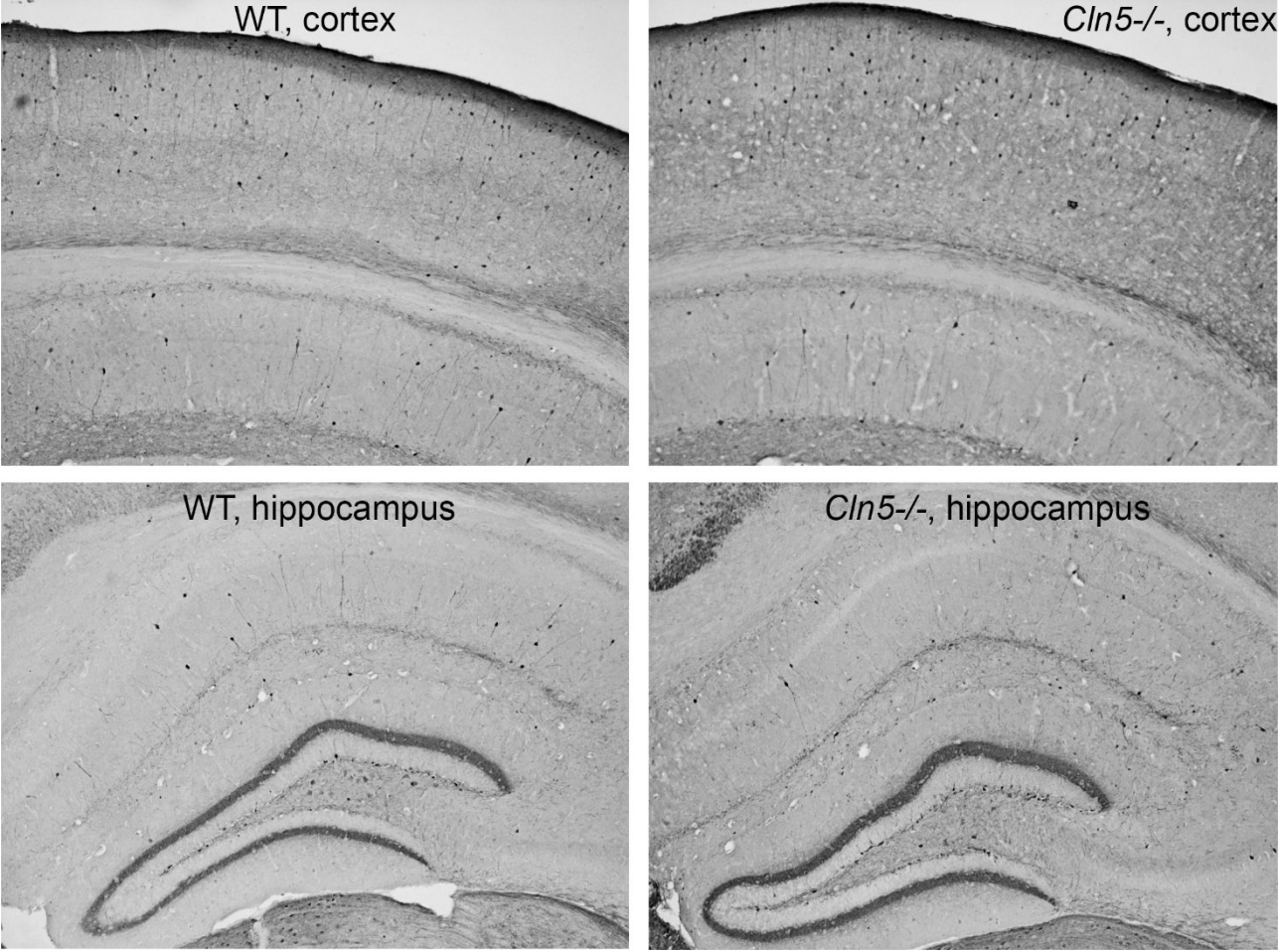
*To add further, the increased TUNEL staining in the dorsal pallium wall likely represents both the neuronal progenitor cells and their neuronal populations. Nonetheless, involvement of some interneurons that have already populated the developing cortex by E14.5 cannot be ruled out. One of the aims of the current study was to explore the hypothesis that neurodegenerative diseases may have their origins during the in utero period (Barker et al. 2002; Barker et al. 2004; Lahti et al. 2010; Lahiri et al. 2009; Marques et al. 2013). It is hypothesized that many in utero developmental insults remain latent which can manifest later into an overt disease at some time point during the postnatal period or adulthood. A number of studies show that an initial insult during early development may result in postnatal brain anomalies (Buka and Fan, 1999; Jaaro-Peled et al. 2009; Silva et al. 2012). In an interesting study by Niwa et al. (2010), a transient knockdown of DISC1 during pre-/peri-natal stages, in a lineage of pyramidal neurons from prefrontal cortex, led to selective abnormalities in postnatal mesocortical dopaminergic maturation and behavioral abnormalities associated with disturbed cortical neurocircuitry after puberty. This study shows an example of early development deficits that affect postnatal brain function and cause behavioral phenotype in adulthood.*

*As a summary, the primary aim of this study was to draw the reader's attention towards the hypothesis that NCLs might have a crucial neurodevelopmental component since NCL associated genes, such as Cln5, show a high expression during the embryonic brain development. It was somewhat beyond the scope of the current study to link these early developmental changes to the brain pathology in adult Cln5<sup>-/-</sup> mice. Instead, we did a few simple experiments to show that the neurological phenotype in Cln5<sup>-/-</sup> mice does not seem to aggravate with age, but rather seem to be acquired congenitally.*

1  
2  
3  
4  
5  
6  
7  
8  
9  
10  
11  
12  
13  
14  
15  
16  
17  
18  
19  
20  
21  
22  
23  
24  
25  
26  
27  
28  
29  
30  
31  
32  
33  
34  
35  
36  
37  
38  
39  
40  
41  
42  
43  
44  
45  
46  
47  
48  
49  
50  
51  
52  
53  
54  
55  
56  
57  
58  
59  
60

**4) When the authors do interneuron counts, they only look at one class of interneurons - - parvalbumin +. However, numerous papers by Cooper et al have shown changes in several different classes of GABAergic interneurons in different forms of Batten disease. Are the authors missing changes in the cortex because of the limited examination.**

*We agree that many different classes of interneurons are affected in CLN disease and as such we also tried to look for other GABAergic neurons in the cortex. The caudal ganglionic eminence (CGE) gives rise to about 30% of interneuronal populations (12) and the major subgroup of calretinin-expressing (CR) interneurons originates mainly from the CGE (13). Since the CGE also showed anomalies in our experiments, we decided to analyze CR immunoreactivity in the adult brain. However, we did not find differences in adult CLN5-KO cortex (Image below).*



*Calretinin immunohistochemistry.*

**5) For much of the histopathology, it is unclear what regions of the cortex the cell counts are being performed in. For instance, loss of GABAergic neurons in other forms of Batten disease has been shown to be associated with limited/distinct functional regions. Again are the authors missing differences because they are not restricting their analysis to particular regions.**

*This is again important comment and well taken by the authors. We indeed carried out analysis of parvalbumin positive cells in a number of different brain areas in the adult brains, including cortex, hippocampus and cerebellum. However, the only significant alterations were found in the CA1 and hilus area of hippocampi.*

With regard to the embryos, we have added a supplementary figure S2 that shows the representative areas of interest where immunoreactivities were calculated in the WT and Cln5-KO embryonic brain sections. In the dorsal telencephalon (dT) the circles show the areas where immunoreactivities were analyzed in 200-400 $\mu$ m wide windows spanning across the entire telencephalic wall. In the ventral telencephalon (vT) the circles show the ganglionic eminences (GEs). The immunoreactivities in the GEs were mainly analyzed in lateral ganglionic eminences (LGE; upper circle in Intermediate section image), medial ganglionic eminences (MGE; lower circle in Intermediate section image) and caudal ganglionic eminence (circle in Caudal section image) in form of circles covering approximately 85000  $\mu$ m<sup>2</sup> area. For IHC analysis, 2-3 anatomically matched sections from the rostral-caudal axis of WT and Cln5-KO embryos were taken. Wherever applicable different layers in the dorsal pallium were identified according to Bayer et al. 1991, based on cell morphology and density identified with a 20X magnification. Mid dorsal pallium region of the embryo brain sections (dT) was visualized using 10x magnification and immunoreactivity per unit area was quantified in the different identified layers or entire telencephalic wall using a 200-400 $\mu$ m wide window with Image-Pro plus 6.0.

**6) For the deficits in neurite outgrowth, does this correlate with any long term consequences in the mice -- ie., inability to form long distance fiber tracts OR are there instance of white matter/DTI imaging deficits in human patients that would result from decreased neuritogenesis?**

The neurite outgrowth assay was carried out in vitro in cultured cells. Therefore, a direct correlation to long-term consequences in vivo is difficult to make, and even more so, in patients. However, our in vitro data on neurite outgrowth provides important mechanistic information that fits with the in vivo findings of the study.

**7) to extend the loss of interneurons to some behavioral deficits, the authors perform a number of behavioral assays. However, how do the auditory measures and rotarod assays performed correlate with loss of interneurons in the hippocampus? Wouldn't a learning and memory assay have been more suitable to correlate with hippocampal defects? Is there a direct circuit from the hippocampus that is involved in these measures?**

Auditory evoked potentials (AEPs) as measured with the midline screw electrodes in rodents are sensitive to auditory gating in the hippocampus. Impaired auditory gating has been considered a measure of interneuron function in the hippocampus (14, 15) We have also observed overall increased AEPs in mice with defective perisomatic nets by interneurons (mainly PV) in cortex and hippocampus (16). The reviewer is right that part of our electrophysiological recordings (cortical EEG) and Rotarod test do not have a direct correlate with interneuron population in the hippocampus. Instead, our electrophysiology data provide evidence of cortical hyper excitability that does not aggravate between 2 and 6 months of age, and thus appears to be acquired congenitally. Decreased inhibitory drive due to defects in the development of cortical interneurons provides a likely explanation for this finding.

Our 9-month rotarod follow-up, started at 1-month of age, strongly suggests that the motor phenotype too is congenitally acquired, and does not significantly progress in Cln5-KO mice. As we did not provide a direct anatomical correlate for this performance defect, we kept the data merely as curiosity and present it as supplementary data.



1  
2  
3  
4  
5  
6  
7  
8  
9  
10  
11  
12  
13  
14  
15  
16  
17  
18  
19  
20  
21  
22  
23  
24  
25  
26  
27  
28  
29  
30  
31  
32  
33  
34  
35  
36  
37  
38  
39  
40  
41  
42  
43  
44  
45  
46  
47  
48  
49  
50  
51  
52  
53  
54  
55  
56  
57  
58  
59  
60

*To assess spatial learning and memory CLN5-KO mice, we performed Morris swim task which showed a significant performance impairment. Unfortunately, however, we cannot draw a solid conclusion whether the performance defect was caused by memory defect or visual impairment. The Cln5-KO mice display a robust retinal degeneration that affect rod-mediated vision from early life, and cone-mediated vision from approximately 5 months of age onwards (11).*

**8) There are number of acronyms in the paper that are never defined -- unless the reader is a neuroscientist, they may never know what these mean (EEG, PSD, AEP, RGC)**

*Abbreviations are now listed in the manuscript.*

**9) There are several images that lack scale bars.**

*Scale bars have now been added.*

**10) Figure 2 legend and labels of figure don't match. TUNEL in legend is A&B but in the actual figure they are last.**

*We thank the reviewer for being observant. This mistake has been now corrected in Fig. 2 legend.*

**REFERENCES**

(1) Lu T, Aron L, Zullo J, Pan Y, Kim H, Chen Y, Yang TH, Kim HM, Drake D, Liu XS, Bennett DA, Colaiácovo MP, Yankner BA. REST and stress resistance in ageing and Alzheimer's disease. Nature. 2014 Mar 27;507(7493):448-54. doi: 10.1038/nature13163.

(2) Ooi L, Wood IC. Chromatin crosstalk in development and disease: lessons from REST. Nat Rev Genet. 2007 Jul;8(7):544-54.

(3) Brennan GP, Dey D, Chen Y, Patterson KP, Magnetta EJ, Hall AM, Dube CM, Mei YT, Baram TZ. Dual and Opposing Roles of MicroRNA-124 in Epilepsy Are Mediated through Inflammatory and NRSF-Dependent Gene Networks. Cell Rep. 2016 Mar 15;14(10):2402-12. doi: 10.1016/j.celrep.2016.02.042.

(4) Calderone A, Jover T, Noh KM, Tanaka H, Yokota H, Lin Y, Grooms SY, Regis R, Bennett MV, Zukin RS. Ischemic insults derepress the gene silencer REST in neurons destined to die. J Neurosci. 2003 Mar 15;23(6):2112-21. PubMed PMID: 12657670.

(5) Palm K, Belluardo N, Metsis M, Timmusk T. Neuronal expression of zinc finger transcription factor REST/NR SF/XBR gene. J Neurosci. 1998 Feb 15;18(4):1280-96. PubMed PMID: 9454838.

(6) Pivtoraiko VN, Stone SL, Roth KA, Shacka JJ. Oxidative stress and autophagy in the regulation of lysosome-dependent neuron death. Antioxid Redox Signal. 2009 Mar;11(3):481-96. doi: 10.1089/ARS.2008.2263.

(7) Wei H, Kim SJ, Zhang Z, Tsai PC, Wisniewski KE, Mukherjee AB. ER and oxidative stresses are common mediators of apoptosis in both neurodegenerative and non-neurodegenerative



- lysosomal storage disorders and are alleviated by chemical chaperones. *Hum Mol Genet.* 2008 Feb 15;17(4):469-77.
- (8) Fiorenza MT, Moro E, Erickson RP. The pathogenesis of lysosomal storage disorders: beyond the engorgement of lysosomes to abnormal development and neuroinflammation. *Hum Mol Genet.* 2018 Aug 1;27(R2):R119-R129.
- (9) Glasgow SM, Henke RM, Macdonald RJ, Wright CV, Johnson JE. Ptf1a determines GABAergic over glutamatergic neuronal cell fate in the spinal cord dorsal horn. *Development.* 2005 Dec;132(24):5461-9.
- (10) Schmiedt ML, Blom T, Blom T, Kopra O, Wong A, von Schantz-Fant C, Ikonen E, Kuronen M, Jauhainen M, Cooper JD, Jalanko A. Cln5-deficiency in mice leads to microglial activation, defective myelination and changes in lipid metabolism. *Neurobiol Dis.* 2012 Apr;46(1):19-29. doi 10.1016/j.nbd.2011.12.009.
- (11) Leinonen H, Keksa-Goldsteine V, Ragauskas S, Kohlmann P, Singh Y, Savchenko E, Puranen J, Malm T, Kalesnykas G, Koistinaho J, Tanila H, Kanninen KM. Retinal Degeneration In A Mouse Model Of CLN5 Disease Is Associated With Compromised Autophagy. *Sci Rep.* 2017 May 9;7(1):1597. doi: 10.1038/s41598-017-01716-1
- (12) Miyoshi G, Hjerling-Leffler J, Karayannis T, Sousa VH, Butt SJ, Battiste J, Johnson JE, Machold RP, Fishell G. Genetic fate mapping reveals that the caudal ganglionic eminence produces a large and diverse population of superficial cortical interneurons. *J Neurosci.* 2010 Feb 3;30(5):1582-94. doi: 10.1523/JNEUROSCI.4515-09.2010.
- (13) Xu Q, Guo L, Moore H, Waclaw RR, Campbell K, Anderson SA. Sonic hedgehog signaling confers ventral telencephalic progenitors with distinct cortical interneuron fates. *Neuron.* 2010 Feb 11;65(3):328-40. doi: 10.1016/j.neuron.2010.01.004.
- (14) Okamoto M, Katayama T, Suzuki Y, Hoshino KY, Yamada H, Matsuoka N, Jodo E. Neonatal administration of phencyclidine decreases the number of putative inhibitory interneurons and increases neural excitability to auditory paired clicks in the hippocampal CA3 region of freely moving adult mice. *Neuroscience.* 2012 Nov 8;224:268-81.
- (15) Miller CL, Freedman R. The activity of hippocampal interneurons and pyramidal cells during the response of the hippocampus to repeated auditory stimuli. *Neuroscience.* 1995 Nov;69(2):371-81.
- (16) Gurevicius K, Gureviciene I, Valjakka A, Schachner M, Tanila H. Enhanced cortical and hippocampal neuronal excitability in mice deficient in the extracellular matrix glycoprotein tenascin-R. *Mol Cell Neurosci.* 2004 Mar;25(3):515-23.

- Barker DJ, Eriksson JG, Forsen T, Osmond C. Fetal origins of adult disease: strength of effects and biological basis. *Int J Epidemiol* 2002 Dec;31(6):1235-1239.
- Barker DJ. The developmental origins of adult disease. *J Am Coll Nutr* 2004 Dec;23(6 Suppl):588S-595S
- Buka SL, Fan AP. Association of prenatal and perinatal complications with subsequent bipolar disorder and schizophrenia. *Schizophr Res*. 1999;39:113–119. discussion 160-111. [[PubMed](#)] [[Google Scholar](#)]
- Burek MJ, Oppenheim RW. Cellular Interactions that Regulate Programmed Cell Death in the Developing Vertebrate Nervous System. In: Koliatsos VE, Ratan RR, editors. *Cell Death and Diseases of the Nervous System* Totowa, NJ: Humana Press; 1999. p. 145-179.
- Guilherme Testa-Silva,<sup>1</sup> Alex Loebel,<sup>2</sup> Michele Giugliano,<sup>3,4,5</sup> Christiaan P.J. de Kock,<sup>1</sup> Huibert D. Mansvelder,<sup>1</sup> and Rhiannon M. Meredith<sup>1</sup>Hyperconnectivity and Slow Synapses during Early Development of Medial Prefrontal Cortex in a Mouse Model for Mental Retardation and Autism. *Cereb Cortex*. 2012 Jun; 22(6): 1333–1342.
- Götz M, Stoykova A, Gruss P. Pax6 controls radial glia differentiation in the cerebral cortex. *Neuron*. 1998 Nov;21(5):1031-44.
- Jaaro-Peled H, Hayashi-Takagi A, Seshadri S, Kamiya A, Brandon NJ, Sawa A. Neurodevelopmental mechanisms of schizophrenia: understanding disturbed postnatal brain maturation through neuregulin-1-ErbB4 and DISC1. *Trends Neurosci*. 2009;32:485–495
- Lahiri DK, Maloney B, Zawia NH. The LEARN model: an epigenetic explanation for idiopathic neurobiological diseases. *Mol Psychiatry* 2009 Nov;14(11):992-1003.
- Lahti J, Raikkonen K, Pesonen AK, Heinonen K, Kajantie E, Forsen T, et al. Prenatal growth, postnatal growth and trait anxiety in late adulthood - the Helsinki Birth Cohort Study. *Acta Psychiatr Scand* 2010 Mar;121(3):227-235.
- Marín O, Rubenstein J.L.R. A long, remarkable journey: Tangential migration in the telencephalon. *Nature Reviews Neuroscience* volume 2, pages780–790 (2001).
- Marques AH, O'Connor TG, Roth C, Susser E, Bjorke-Monsen AL. The influence of maternal prenatal and early childhood nutrition and maternal prenatal stress on offspring immune system development and neurodevelopmental disorders. *Front Neurosci* 2013 Jul 31;7:120.
- McNeil TF. Perinatal risk factors and schizophrenia: selective review and methodological concerns. *Epidemiol Rev*. 1995;17:107–112.
- Minae Niwa et al. Knockdown of DISC1 by in utero gene transfer disturbs postnatal dopaminergic maturation in the frontal cortex and leads to adult behavioral deficits. *Neuron*. 2010 Feb 25; 65(4): 480–489
- Rabinowicz T, de Courten-Myers GM, Petetot JM, Xi G, de los Reyes E. Human cortex development: estimates of neuronal numbers indicate major loss late during gestation. *J Neuropathol Exp Neurol* 1996 Mar;55(3):320-328.

1  
2  
3 Rakic S, Zecevic N. Programmed cell death in the developing human telencephalon. *Eur J Neurosci*  
4 2000 Aug;12(8):2721-2734.  
5

6  
7 Roseboom TJ, van der Meulen JH, Ravelli AC, Osmond C, Barker DJ, Bleker OP. Effects of prenatal  
8 exposure to the Dutch famine on adult disease in later life: an overview. *Mol Cell Endocrinol* 2001  
9 Dec 20;185(1-2):93-98. 132  
10

11 Lahiri DK, Maloney B, Zawia NH. The LEARN model: an epigenetic explanation for idiopathic  
12 neurobiological diseases. *Mol Psychiatry* 2009 Nov;14(11):992-1003.  
13  
14  
15  
16  
17  
18  
19  
20  
21  
22  
23  
24  
25  
26  
27  
28  
29  
30  
31  
32  
33  
34  
35  
36  
37  
38  
39  
40  
41  
42  
43  
44  
45  
46  
47  
48  
49  
50  
51  
52  
53  
54  
55  
56  
57  
58  
59  
60

For Peer Review

**Loss of *Cln5* leads to altered *Gad1* expression and deficits in interneuron development in mice**

Yajuvinder Singh<sup>1#</sup>, Henri Leinonen <sup>1,2#</sup>, Feroze Fazaludeen <sup>1</sup>, Merja Jaronen <sup>1</sup>, Debbie Guest <sup>3</sup>, Noel Buckley <sup>4</sup>, Nadiya Byts <sup>5</sup>, Petra Oksa <sup>1</sup>, Kari Jalkanen <sup>1</sup>, Imran Iqbal<sup>1</sup>, Mikko Huuskonen <sup>1</sup>, Ekaterina Savchenko <sup>1</sup>, Velta Keksa-Goldsteine <sup>1</sup>, Sweelin Chew <sup>1</sup>, Johanna Myllyharju <sup>5</sup>, Heikki Tanila <sup>1</sup>, Lezanne Ooi <sup>6</sup>, Jari Koistinaho <sup>1</sup>, Katja M. Kanninen <sup>1§</sup>, Tarja Malm <sup>1§\*</sup>.

<sup>1</sup>A. I. Virtanen Institute for Molecular Sciences, University of Eastern Finland, Kuopio, Finland

<sup>2</sup>Department of Ophthalmology, School of Medicine, University of California Irvine, Irvine, Ca, USA.

<sup>3</sup>Animal Health Trust, Lanwades Park, Kentford, Newmarket, Suffolk CB8 7UU, United Kingdom.

<sup>4</sup>Department of Psychiatry, University of Oxford, Warneford Hospital, Oxford, OX3 7JX, United Kingdom.

<sup>5</sup>Oulu Centre for Cell Matrix Research, Biocenter Oulu and Faculty of Biochemistry and Molecular Medicine, University of Oulu, Oulu, Finland

<sup>6</sup>Illawarra Health and Medical Research Institute, School of Biological Sciences, University of Wollongong, Wollongong, NSW, 2522, Australia.

# equal contribution

§ equal contribution

**Address correspondence to:**

\*Tarja Malm

A.I.Virtanen Institute for Molecular Sciences

University of Eastern Finland

Yliopistonranta 1, 70210, Kuopio, Finland.

Phone: +358 40 3552209

Email: [Tarja.malm@uef.fi](mailto:Tarja.malm@uef.fi)



## Abstract

The Finnish variant Late Infantile Neuronal Ceroid Lipofuscinosis (vLINCL<sub>Fin</sub>), also known as CLN5 disease, is caused by mutations in the *CLN5* gene. *Cln5* is strongly expressed in the developing brain and expression continues into adulthood. CLN5, a protein of unknown function, is implicated in neurodevelopment but detailed investigation is lacking. Using *Cln5*<sup>-/-</sup> embryos of various ages and cells harvested from *Cln5*<sup>-/-</sup> brains we investigated the hitherto unknown role of *Cln5* in the developing brain. Loss of *Cln5* results in neuronal differentiation deficits and delays in interneuron development during *in utero* period. Specifically, the radial thickness of dorsal telencephalon was significantly decreased in *Cln5*<sup>-/-</sup> mouse embryos at embryonic day 14.5 (E14.5), and expression of Tuj1, an important neuronal marker during development, was down-regulated. An interneuron marker calbindin and a mitosis marker p-H3 showed down-regulation in ganglionic eminences. Neurite outgrowth was compromised in primary cortical neuronal cultures derived from E16 *Cln5*<sup>-/-</sup> embryos compared to WT embryos. We show that the developmental deficits of interneurons may be linked to increased levels of the Repressor Element 1-Silencing Transcription factor (REST), which we report to bind to *Gad1*, which encodes glutamate decarboxylase (GAD) 67, a rate-limiting enzyme in the production of GABA. Indeed, adult *Cln5*<sup>-/-</sup> mice presented deficits in hippocampal parvalbumin-positive interneurons. Furthermore, adult *Cln5*<sup>-/-</sup> mice showed age-independent cortical hyper excitability as measured by electroencephalogram and auditory-evoked potentials. This study highlights the importance of *Cln5* in neurodevelopment and suggests that in contrast to earlier reports, CLN5 disease is likely to develop during embryonic stages.

**Introduction**

The neuronal ceroid lipofuscinoses (NCLs) constitute a group of inherited lysosomal storage disorders and the most common group of pediatric neurodegenerative disorders (1). Depending on geography and ancestry the incidence of NCLs varies from 1:8000 to 1:100000 (2, 3) and is highest in the Nordic countries (4). Most NCLs are inherited in an autosomal recessive manner, but some patients with adult NCL variants show autosomal dominant inheritance (5). Currently, 13 genetically distinct human NCLs variants have been identified (6). The childhood forms of NCLs are generally characterized by cognitive and motor deficits, progressive loss of vision, epileptic seizures and premature death (7), while the more rare adult-onset forms are dominated by dementia. Pathological hallmarks of NCLs include progressive neurodegeneration, massive glial activation, and accumulation of auto-fluorescent storage material within lysosomes both in the central nervous system (CNS) and the periphery.

CLN5 disease, also called Finnish variant Late Infantile Neuronal Ceroid Lipofuscinosis (vLINCL<sub>Fin</sub>), results from mutations in the *CLN5* gene. CLN5 disease has an onset at approximately 2–7 years of age and because no cure exists, culminates in death between 14–36 years of age (8). To date, 37 disease causing mutations in the *CLN5* gene have been documented (9). Although the exact role of CLN5 remains unknown, it is well accepted that it is a lysosome trafficked soluble glycoprotein (10, 11). Similar to other NCL forms, *CLN5* deficiency is pathologically characterized by the accumulation of lysosomal auto-fluorescent material in both the CNS and the peripheral tissues (3, 12, 13).

It has been speculated that CLN5 is involved in neurodevelopment. In a pioneering study, Heinonen et al. (14) reported that *CLN1* and *CLN5* genes are expressed in the embryonic brain

between 37 to 84 days post fertilization, and that the expression of these genes increases during development. The expression of *CLN1* and *CLN5* is observed in different zones of dorsal telencephalon including the subventricular zone (SVZ), intermediate zone (IZ) and cortical plate (CP), which house the stem cells and migrating and differentiating neuronal populations, respectively. In the mouse brain, *Cln5* is ubiquitously expressed in the entire brain at embryonic day 15 (E15) and peaks at approximately postnatal day 30 (P30) (10). Furthermore, high *Cln5* expression is observed in the cerebral cortex, cerebellum and ganglionic eminences (GEs) of the embryonic brain. In contrast, the cerebellar Purkinje cell layer and the hippocampus are the main sites of high *Cln5* expression in the adult mouse brain (10). The diverse spatial and temporal expression of *Cln5* in the different germinative areas of the developing and adult brain suggests that *Cln5* may have a broad role in both embryonic brain development and maintenance of adult brain function. To date, there is no knowledge of the exact role of *Cln5* in neurodevelopment.

We show here for the first time that loss of *Cln5* triggers alterations in development and defects in embryonic interneurons. This may occur through increased binding of REST to *Gad1*, which encodes a rate limiting enzyme for GABA in interneurons (15). This study presents evidence that CLN5 functions as a critical modulator of key parameters required for proper neuronal development and maturation, and that the neurodegenerative processes of CLN5 disease pathophysiology have a neurodevelopmental component.

**Results**

**Loss of *Cln5* leads to developmental cytoarchitectural changes and perturbations in stem cell populations in the dorsal telencephalon**

To investigate neuronal development and cytoarchitecture, brains from *Cln5*<sup>-/-</sup> embryos and WT controls at E14.5 were stained with Cresyl Violet. ~E14.5 is a time point when *Cln5* is ubiquitously expressed in the developing brain and it is the peak of neurogenesis in the mouse embryo. Nissl staining revealed a significant reduction in the radial thickness along the rostro-caudal axis of approximately 31% ( $t_9 = 4.0$ ,  $P<0.01$ ), 27% ( $t_{10}=3.1$ ,  $P<0.05$ ) and 28% ( $t_9=3.2$ ,  $P<0.05$ ) in the *Cln5*<sup>-/-</sup> embryos along the rostral, intermediate and caudal sections, respectively, when compared to WT mice (Fig. 1A-I).

First we investigated whether changes in proliferation, differentiation and/or apoptosis could explain the observed architectural alterations in the E14.5 *Cln5*<sup>-/-</sup> embryos. Quantification of Pax6 immunoreactivity showed a significant increase of 45% ( $t_9=2.2$ ,  $P<0.05$ ) in the intermediate and 73% ( $z=-2.11$ ,  $P<0.05$ ) in the caudal forebrain of the *Cln5*<sup>-/-</sup> embryos when compared to their age-matched WT controls (Fig. 1N).

We next examined the differentiation fate of neurons in the wall of the dorsal telencephalon immunohistochemically using Tuj1 as a marker for one of the earliest neuronal populations (16). The Tuj1 immunoreactivity in the CP was significantly reduced in E14.5 *Cln5*<sup>-/-</sup> embryos (rostral:  $z=2.3$ ,  $P<0.05$ ; intermediate:  $t_{10}=2.7$ ,  $P<0.05$ ; caudal:  $t_{10}=2.9$ ,  $P<0.05$ ) (Fig 1O). On the other hand, the extent of nestin immunoreactivity was not significantly different ( $P\geq 0.09$ ) between the genotypes in any of the regions analyzed (SI appendix Fig. S1 & S2). In contrast to E14.5,



alterations in the extent of Tuj1 and Pax6 immunoreactivities were no longer evident at E17.5 in *Cln5*<sup>-/-</sup> brains (SI appendix Fig. S3) indicating primarily delayed *in utero* development.

### **Increased apoptosis and altered stem cell proliferation in dorsal telencephalon of E14.5 *Cln5*<sup>-/-</sup> embryos**

To investigate whether loss of *Cln5* interferes with the rate of apoptosis, we analyzed the *Cln5*<sup>-/-</sup> and WT embryos by the TUNEL assay (Fig. 2A-B). Indeed, the number of apoptotic cells in the dorsal telencephalon was significantly higher in E14.5 *Cln5*<sup>-/-</sup> embryonic brains than in WT controls (Fig. 2C,  $t_5=3.0$ ,  $P<0.05$ ).

We next analyzed if there are any changes in the proliferation rate of the stem cell populations in the dorsal telencephalon by using p-H3 as a marker for mitosis (Fig. 2D-F). Quantification of p-H3 immunoreactivity revealed a nearly significant increase in the intermediate (Fig. 2E,  $t_9=2.2$ ,  $P=0.06$ ) and a significant increase in the caudal (Fig. 2F,  $t_{10}=2.24$ ,  $P<0.05$ ) parts of the dorsal telencephalon, corresponding to the area where Pax6 immunoreactivity was observed earlier.

### **Loss of *Cln5* affects stem cell proliferation rate and interneuron populations in the ganglionic eminences**

As a number of previous studies have shown that NCL proteins (17, 18) including *Cln5* are involved in functioning of interneurons (19) we next assessed whether *Cln5* could be implicated in interneuron development during embryonic stages. We stained E14.5 embryonic brain sections against calbindin, a marker for early interneurons, and quantified immunoreactivity at the site of interneuron birth, *i.e.* at the GEs (Fig 3A-D). Quantification at the principal source of interneurons

during this period, *i.e.* medial GE (MGE), showed a significant 68% decrease in immunoreactivity in the *Cln5*<sup>-/-</sup> embryos (Fig. 3C,  $t_8=3.3$ ,  $P<0.05$ ). However, the decrease in the calbindin immunoreactivity did not reach a statistical significance level in the lateral GE (LGE; Fig. 3D,  $t_{10}=1.9$ ,  $P=0.09$ ). Calbindin immunoreactivity in the dorsal telencephalon did not show any alterations in *Cln5*<sup>-/-</sup> embryos (SI appendix Fig. S4).

Then, we tested if changes in the proliferation rate of the stem cell populations in the ventral telencephalon could potentially play a role in the interneuronal loss observed in the GEs of *Cln5*<sup>-/-</sup> embryos. Quantification of p-H3 positive cells in the GEs revealed a nearly significant reduction in the mitotic cell count in the MGE (Fig. 3I,  $z=1.8$ ,  $P=0.07$ ) and significant reductions in the LGE (Fig. 3J;  $z=2.5$ ,  $P<0.01$ ) and caudal GE (CGE; Fig. 3K,  $t_{10}=2.5$ ,  $P<0.05$ ) in *Cln5*<sup>-/-</sup> embryos.

We also investigated whether the loss of *Cln5* influences the tangential migration of interneurons from the GEs to the dorsal telencephalon. We analyzed the flux of calbindin immunoreactive cells at the junction of the dorsal telencephalon and ventral telencephalon representing the outflow of interneurons migrating towards various regions of the upper brain from their origin in the GEs. Quantification revealed no differences between genotypes (SI appendix Fig. S5), suggesting that the loss of *Cln5* was unlikely to affect the migration of interneurons towards the dorsal telencephalon. In conclusion, loss of *Cln5* seems to affect interneuron populations of the GEs only.

**Reduced number of interneurons in the adult *Cln5*<sup>-/-</sup> brain**

We next investigated whether the observed deficits in the number of developing interneurons during development persist to an adult age. Although loss of interneurons has been reported in

adult *Cln5*<sup>-/-</sup> mice (13), we are not aware of any attempt to quantify the loss. We therefore analyzed 6-month-old WT and *Cln5*<sup>-/-</sup> mouse brains stained with calcium binding protein parvalbumin (PV), one of the well-known markers for the adult brain interneurons. Although we did not detect differences in the numbers of PV positive interneurons in cortex ( $t_{11}=0.6$ ,  $P=0.5$ , data not shown), we found significant reductions in the numbers of PV interneurons in the CA1 (Fig. 4A-C,  $t_{11}=3.7$ ,  $P<0.01$ ) and hilar regions (Fig. 4D-F,  $t_{14}=3.0$ ,  $P<0.01$ ) of adult *Cln5*<sup>-/-</sup> hippocampi.

### Loss of *Cln5* suppresses neurite outgrowth

Neurite outgrowth, one of the key aspects of the developmental chain of events in the brain, can be recapitulated under *in vitro* conditions by primary neural cultures from the developing brain. Thus, we studied the differentiation-related morphological changes in primary cortical neurons derived from *Cln5*<sup>-/-</sup> and WT mice by time-lapse microscopy. The live-cell imaging results demonstrate the formation of an extensive neurite network in WT neurons that were accompanied by high neurite length and branching points (Fig. 5A). In contrast, *Cln5*<sup>-/-</sup> neurons appeared to exhibit fewer and shorter neurite-like extensions (Fig. 5B). Indeed, neuronal outgrowth was suppressed in *Cln5*<sup>-/-</sup> cortical neurons as shown by reduced gain of neurite length as compared to WT neurons (Fig. 5C,  $F_{1,4}=9.0$ ,  $P<0.05$ ). However, quantified neurite branching analysis showed no difference in the number of branching points between the *Cln5*<sup>-/-</sup> and WT cells (data not shown).

### REST is up-regulated in *Cln5*<sup>-/-</sup> brains

Our previous study showed that *Cln5*<sup>-/-</sup> mice exhibit impaired neurogenesis (20). Since the repressor element 1-silencing transcription factor (REST), also called neuron-restrictive silencing factor (NRSF) is a master regulator of neurogenesis, we next evaluated whether REST is

implicated in the observed changes in *Cln5*<sup>-/-</sup> mice. Whereas the mRNA levels of REST in the cortical samples of *Cln5*<sup>-/-</sup> E14.5 embryos were unaltered ( $t_{13} = 0.19$ ,  $P=0.85$ , data not shown), increased REST protein levels were detected in *Cln5*<sup>-/-</sup> hippocampi at the age of 6 months (Fig. 6A, B,  $t_{11}=2.2$ ,  $P<0.05$ ).

**REST regulates genes involved in the development of GABAergic interneurons**

To evaluate the genes that REST regulates in neural stem cells, we carried out a ChIP microarray in NS5 cells (Table 1 and SI appendix Table S1). The array revealed that REST regulates genes that are critical for GABAergic development. We thus validated these genes by ChIP-qPCR and confirmed that in neural stem cells REST regulates *Gad1* and *Ptf1a*, two genes that are important in the development of GABAergic interneurons, along with well-characterised REST target genes, such as *Tubb3* (Fig. 6C). *Gad1* mRNA expression was not altered in total hippocampal samples (data not shown). GAD67 is the enzyme responsible for the conversion of glutamic acid to GABA in interneurons and is controlled by the transcription factor Ptf1a (20,21). The NS5 neural stem cells are known to express telencephalic markers and generate GABAergic, GAD67 positive neurons upon differentiation (22). To further evaluate the involvement of REST in regulating these genes, REST function was inhibited by overexpressing dominant negative REST (DN:REST) in NS5 cells. Indeed, Ptf1a was silent in control cells and the overexpression of DN:REST induced the expression of *Ptf1a* in NS5 cells, indicating that REST is responsible for silencing this gene in these cells (Fig. 6D). To verify the interaction of REST and *Gad1* in tissues *in vivo*, we carried out ChIP-qPCR analysis of hippocampal samples from 5-month-old *Cln5*<sup>-/-</sup> mice and their WT controls. The analysis showed significantly increased binding of REST with *Gad1* in *Cln5*<sup>-/-</sup> mice ( $z=2.10$ ,  $P<0.05$ , Fig. 6E), consistent with the increased protein expression of REST (Fig. 6A, B).



Table 1. Selected highly enriched genes in ChIP microarray in NS5 cells. Full table showing all genes with > 2-fold mean enrichment is shown in SI appendix Table S1.

Gene	Protein/Function	Mean enrichment	STD
<i>L1cam</i>	Neural cell adhesion molecule L1	44.61	63.965
<i>Rnaseh2a</i>	Ribonuclease H2 subunit A	28.924	26.371
<i>Celf4</i>	Elav-like family member 4, RNA-binding	27.43	21.43
<i>Snap25</i>	Synaptosomal-associated protein 25	20.382	15.483
<i>Syt7</i>	Synaptotagmin-7	20.059	18.944
<i>Cacna1b</i>	Voltage-dependent Ca <sup>2+</sup> channel, N type, $\alpha$ 1B subunit	11.116	8.976
<i>Gad1</i>	Glutamate decarboxylase 1	10.372	7.974
<i>Meis3</i>	Homeobox protein Meis3, transcriptional regulator	9.76	6.098
<i>Tubb3</i>	Tubulin beta-3 chain	6.184	4.972
<i>Ptf1a</i>	Pancreas transcription factor 1 subunit alpha	2.695	2.396

### ***Cln5* deficiency leads to enhanced auditory-evoked potentials**

To determine whether the observed deficits in the interneuron development have functional consequences in adult mice, we measured auditory evoked potentials (AEPs) and auditory gating that are established methodologies to assess short- and long-latency inhibitory mechanism *in vivo* and indicative of interneuronal integrity (21-23). The *in vivo* electrophysiology was performed in awake, head-restrained mice implanted with chronical electrode assembly. The test tone (the second tone of the tone-pair) evoked a clearly suppressed response compared to conditioning tone regardless of mouse genotype or gender (compare Fig. 7 A vs. B and C vs. D). The test tone/conditioning tone amplitude ratio revealed that the response inhibition was decreased in 2-month-old *Cln5*<sup>-/-</sup> mice compared to their age-matched controls (genders pooled:  $F_{1,35}=3.1$ ,  $P=0.09$ ; 2-months:  $t_{35}=2.5$ ,  $P<0.05$ ) (Fig. 7F). In other words, the auditory gating was slightly impaired in young adult *Cln5*<sup>-/-</sup> mice.

### ***Cln5*<sup>-/-</sup> male mice show increased electroencephalogram (EEG) power spectral density**

Brain hyperexcitability may be a consequence of imbalance between brain excitability and inhibition and may be observed in EEG recordings as increased power spectral density (PSD), especially in the gamma band. We performed PSD analysis (*i.e.* EEG power at different frequency

bands) from EEG signal collected consecutively for 5 min in still head-fixed *Cln5*<sup>-/-</sup> and WT mice. The PSD was increased in male *Cln5*<sup>-/-</sup> mice at all frequency ranges at both 2 months (Fig. 7G; theta:  $t_{11}=3.2$ ,  $P<0.01$ ; alpha:  $t_{11}=2.9$ ,  $P<0.05$ ; beta:  $t_{11}=4.1$ ,  $P<0.01$ ; gamma:  $t_{11}=4.8$ ,  $P<0.001$ ) and at 6 months of age (Fig 7H; theta:  $t_{10}=2.8$ ,  $P<0.05$ ; alpha:  $t_{10}=3.0$ ,  $P<0.05$ ; beta:  $t_{10}=4.1$ ,  $P<0.01$ ; gamma:  $t_{10}=3.8$ ,  $P<0.01$ ). In contrast, female *Cln5*<sup>-/-</sup> mice displayed similar PSD as their gender-matched controls (Fig. 7I-J). ANOVA for repeated measures revealed no age effect in PSDs between 2 and 6 months of age (WT male:  $F_{1,8}=0.1$ ,  $P=0.74$ ; *Cln5*<sup>-/-</sup> male:  $F_{1,12}=1.3$ ,  $P=0.28$ ; WT female:  $F_{1,12}=0.5$ ,  $P=0.50$ ; *Cln5*<sup>-/-</sup> female:  $F_{1,14}=0.4$ ,  $P=0.56$ ).

**Loss of *Cln5* leads to impaired motor coordination and balance**

Since motor deterioration is a key hallmark of NCLs (7) and hypomyelination has been previously described in *Cln5*<sup>-/-</sup> mice (24), we were interested in seeing if *Cln5*<sup>-/-</sup> mice display a motor phenotype and if it is progressive in nature. To this end, we performed a longitudinal motor performance follow-up by Rotarod test (25) from 1 to 10 months of age. Both male and female *Cln5*<sup>-/-</sup> mice performed worse than their sex-matched controls in the Rotarod test regardless of age (SI Appendix Fig. 6). We pooled results from male and female mice for statistical analysis due to small group sizes and similar results between the genders. The performance difference between genotypes was significant across all the tested ages and did not aggravate over time ( $F_{1,90}=108.8$ ,  $P<0.001$ ).

## 260 Discussion

261 Previous studies have shown that NCL associated *CLN2*, *CLN3* and *CLN5* genes are active in  
262 multipotent neurospheres (26). Moreover, at E14.5, *Cln5* is widely distributed in the developing  
263 brain with a high expression in the highly proliferative areas like the ventricular zone (VZ) (10).  
264 In the current study, E14.5 *Cln5*<sup>-/-</sup> embryos displayed cytoarchitectural deficits in the brain,  
265 suggesting that loss of *Cln5* also affects stem cell populations and their differentiation potential.  
266 As a further indication of abnormal neuronal development, primary neurons cultured from *Cln5*<sup>-/-</sup>  
267 mice showed impaired process formation.

268  
269 Our analysis revealed an increase in the Pax6 positive cells in VZ/SVZ in the caudal brain sections  
270 of *Cln5*<sup>-/-</sup> mice. An increase in the Pax6 immunoreactivity in *Cln5*<sup>-/-</sup> embryos can be due to several  
271 reasons such as deficits in radial glial scaffolds, proliferative deficits, apoptosis, cell fate choice or  
272 a combination of these factors. We did not observe any changes in the radial glial morphology as  
273 observed by nestin staining, which is another neural stem/progenitor cell marker. This suggests  
274 that radial glial fibers are functionally normal in *Cln5*<sup>-/-</sup> embryos. However, we observed a strong  
275 trend towards an increase in the p-H3 counts in the dorsal telencephalon in *Cln5*<sup>-/-</sup> embryos at  
276 E14.5 despite being unable to produce a double staining for Pax6 and p-H3. Nevertheless, our data  
277 suggests that Pax6 increase was most likely due to an increase in the proliferative activity of the  
278 progenitor cells in the *Cln5*<sup>-/-</sup> embryos. Nestin immunoreactivity did not show any expression  
279 differences between *Cln5*<sup>-/-</sup> and WT embryos in our cohort. In the developing brain virtually all  
280 Pax6<sup>+</sup> cells are also positive to nestin, as shown by Götz et al. (27). However, the authors also  
281 show that there is a significant proportion of cells that are nestin positive but Pax6 negative. Thus,  
282 this nestin positive but Pax6 negative but population could overcome the observed difference in  
283 the extent of Pax6 positive and nestin positive cell populations observed in our study.

1  
2  
3  
4  
5  
6  
7  
8  
9  
10  
11  
12  
13  
14  
15  
16  
17  
18  
19  
20  
21  
22  
23  
24  
25  
26  
27  
28  
29  
30  
31  
32  
33  
34  
35  
36  
37  
38  
39  
40  
41  
42  
43  
44  
45  
46  
47  
48  
49  
50  
51  
52  
53  
54  
55  
56  
57  
58  
59  
60

Furthermore, earlier studies have suggested that Pax6 expression has to be “turned off” for proper neuronal differentiation (28). It is plausible that in the absence of *Cln5*, the progenitor cells are unable to downregulate Pax6 levels and remain in a “pre-differentiated” state, leading to altered neuronal differentiation. This idea is corroborated by the findings that *Cln5*<sup>-/-</sup> mice exhibit a reduced amount of β-tubulin in the cortex, as well as in primary embryonic cortical neurons (29). Therefore, *Cln5* may be implicated in the maintenance of the microtubular components of the cytoskeleton and in stem cell functioning in the neurogenic compartments of the developing brain. An earlier study found no direct correlation between neuronal loss and timing or distribution of lipofuscin accumulation in *Cln5*<sup>-/-</sup> mice (30), suggesting that the neuronal loss cannot be explained by disease progression upon aging. In support of this, our study now suggest that these alterations may be initiated already during embryonic developmental stages, although we cannot exclude the possibility that loss of *Cln5* causes a delay rather than a permanent disturbance in the development.

Involvement of apoptotic cascades in NCL pathogenesis has been substantiated by TUNEL positive cells in the brains of LINCL and juvenile NCL (JNCL) patients (31), and in a mouse model of infantile NCL (32). CLN5 in conjunction with CLN3 may regulate cellular apoptosis through regulation of lysosomal pH (33) and dysregulation of sphingolipid metabolism (34), which is also known for CLN2/3/6/8 NCL subtypes (31). We show that the number of TUNEL positive cells is increased in the *Cln5*<sup>-/-</sup> embryos at E14.5, suggesting that the apoptosis is excessively activated at an early developmental stage in *Cln5*<sup>-/-</sup> mice. Therefore, the altered neuronal differentiation observed in our study may result either from an increase in the apoptosis of the differentiating/migrating neurons and/or the inability of the stem cells to undergo normal

306 differentiation in the absence of *Cln5*. Our previous report on altered differentiation of *Cln5*  
307 deficient NPCs (20) support the latter hypothesis.

308  
309 MGE and CGE are the main sources of cortical and hippocampal interneurons (35, 36). Here we  
310 report that loss of *Cln5* affects the interneuron populations of the developing brain. Loss of  
311 calbindin positive interneurons in the E14.5 *Cln5*<sup>-/-</sup> GEs was also accompanied by a reduction in  
312 cellular proliferation. Despite the inability of the current study to determine the state of various  
313 precursor cell markers in the GEs, it is likely that the loss of calbindin results from a reduced  
314 proliferation rate of the resident progenitor populations. GABAergic neurons are affected in NCL  
315 disease pathogenesis in various animal models (17) and humans patients (18). Our study provides  
316 the first evidence that the loss of interneurons in *Cln5*<sup>-/-</sup> mice (13) may indeed be of developmental  
317 origin. Since *Cln5* has a high expression in GEs (10), changes in calbindin immunoreactivity might  
318 actually signal selective early vulnerability of interneurons and may increase susceptibility to  
319 neurodegeneration.

320  
321 We propose that deficits in interneuron development during *Cln5* deficiency arise from increased  
322 levels of REST, leading to enhanced binding of REST to *Gad1* and *Ptf1a*, thus repressing the  
323 production of GABA. Although we do not have direct proof of this *in vivo*, we suggest a novel  
324 model whereby under WT conditions REST expression is down-regulated during GABAergic  
325 neuron development, relieving repression of *Ptf1a* and *Gad1*. REST, which is increased in *Cln5*  
326 deficiency, is bound to the RE1 sites of *Ptf1a* and *Gad1*, resulting in their silencing and reduced  
327 GABAergic neuronal differentiation. The loss of REST from the RE1 site of *Gad1* allows the  
328 expression of this gene and subsequent conversion of glutamic acid into GABA. *Cln5*<sup>-/-</sup> mice



1  
2  
3  
4  
5  
6  
7  
8  
9  
10  
11  
12  
13  
14  
15  
16  
17  
18  
19  
20  
21  
22  
23  
24  
25  
26  
27  
28  
29  
30  
31  
32  
33  
34  
35  
36  
37  
38  
39  
40  
41  
42  
43  
44  
45  
46  
47  
48  
49  
50  
51  
52  
53  
54  
55  
56  
57  
58  
59  
60

exhibit significantly increased levels of REST, without evident re-distribution between the nucleus and cytoplasm (data not shown), which possibly impairs neuronal subtype specification, leading to deficits in interneuron numbers. This is consistent with a coherent type 2 feed-forward loop (37). A feed-forward loop such as this would enable a delay in the response of Gad1 to changes in REST levels, which may be of importance in maintaining normal neuronal functions if REST levels are only transiently affected. While our data does not provide direct evidence that REST is controlling the production of GABAergic interneurons *in vivo*, we demonstrate the direct interaction of REST with Gad1 both *in vitro* and *in vivo*, adding further proof for the involvement of REST in interneuron development. Taking into account the loss of interneurons in adult *Cln5*<sup>-/-</sup> deficient mice, it is plausible that REST is involved in the process of neuronal subtype specification and interneuron differentiation via its control of Gad1. Furthermore, our *in vitro* ChIP-qPCR data revealed that REST also interacts with TUBB3, which encodes Tuj-1. Thus, an increase in REST may also be responsible for the decrease in Tuj-1 that we observed in *Cln5*<sup>-/-</sup> mice. Indeed, REST has been shown to regulate a number of genes associated with GABAergic neurons (38). Taken together, we propose that the loss of the lysosomal protein Cln5 increases inflammation and oxidative stress, leading to an upregulation of REST and a consequent downregulation of genes required for GABAergic differentiation. Importantly, we show for the first time that this may occur through direct interaction of REST with Gad67.

Further evidence for impaired interneuron function comes from electrophysiological recordings in adult *Cln5*<sup>-/-</sup> mice. Impaired auditory gating in female and male *Cln5*<sup>-/-</sup> mice and overall increased power spectral density of the male *Cln5*<sup>-/-</sup> mice all are compatible with decreased inhibition of principal neurons by GABAergic interneurons (21). Impaired auditory gating reflects neural

processing in the so-called extralemniscal pathway rather than the mainstream processing from brainstem auditory nuclei via medial geniculate nucleus to the auditory cortex. The most robust auditory gating is recording in the CA3 field of the hippocampus with local microelectrodes while the gating response via volume conduction can be also seen with parietal screw electrodes (39) as in our study. Thus our finding of reduced auditory gating in *Cln5*<sup>-/-</sup> mice is well in agreement with the observed PV<sup>+</sup> interneuron loss in area CA3 of hippocampus. At present we do not have an explanation as to why only male *Cln5*<sup>-/-</sup> exhibit such a hyperexcited EEG spectra, but females do not. However, males and females have been shown to have estrogen induced differences in hyperexcitability (40). Thus, estrogen could suppress the hyperexcitability in *Cln5*<sup>-/-</sup> females. Interestingly, REST has been shown to regulate also a vast number of genes associated with estrogen signaling (38).

NCLs have been classically categorized as lysosomal storage diseases with a neurodegenerative component manifesting as progressive neuronal loss and behavioral deficits. Here we provide evidence that already during early embryonic development *Cln5*<sup>-/-</sup> mice show alterations in neuronal cytoarchitecture which translates during the postnatal period to a loss of the interneuron populations. It is noteworthy that surrogate markers of interneuron deficits (brain hyperexcitability) in our study do not aggravate over time. Similarly, a major clinical hallmark of NCLs, motor dysfunction, did not aggravate over time as shown by 10-month long Rotarod follow-up. Although earlier studies have revealed a generalized early myelinization defect in *Cln5*<sup>-/-</sup> mice (24), it is difficult to assess the contribution of hypomyelination to behavior, since additional pathological changes such as neuroinflammation are usually present in induced hypomyelination models. It is, however, possible that the demyelination contributes to the observed impairment

in the Rotarod test that draws on fast communication between the cerebellum and spinal cord via long myelinised axons. Nevertheless, these data are in line with our previous study showing that impairment in electroretinographic response arising from the eye’s retinal pigmented epithelium (RPE) in *Cln5*<sup>-/-</sup> mice do not aggravate upon aging (41). These data suggest that the major neurological symptoms in *Cln5*<sup>-/-</sup> mice may be destined from the pre-birth periods.

Pathogenic events underlying NCLs may be initiated prenatally (42, 43). Our study is the first to show that *Cln5* loss of function leads to significant alterations in the development of embryonic mouse brain. Our findings pose two important questions. Firstly, could malfunction of *Cln5* during early embryonic development set the conditions for disease initiation, which over a period of time escalates to form the pathological basis of the disease? Secondly, could *in utero* intervention provide a novel window of opportunity for effective therapeutic intervention for the dreaded NCLs.

**Materials and methods**

**Animals**

The *Cln5*<sup>-/-</sup> model was created by gene targeting using insertion of neomycin selectable marker for the disruption of exon 3. The mice were crossbred to C57BL/6J RccHsd background and C57BL/6J RccHsd mice were used as WT controls (WT). *Cln5*<sup>-/-</sup> mice were a kind gift from Anu Jalanko (13). The embryos were isolated from gravid females at time points E14.5 and E17.5 during the gestation period. For *Cln5*<sup>-/-</sup> mice and their WT counterparts the day when vaginal plug was detected was designated as E0.5. In addition, adult, 2-10 -month-old adult *Cln5*<sup>-/-</sup> mice and their age matched WT counterparts were included in the study. All experimental procedures were

performed in accordance with the European and Finnish legislations for handling and care of laboratory animals and approved by the Animal Experimental Board in Finland.

### **Immunohistochemistry**

The embryo heads were processed as described by Utriainen *et al.* (44). Briefly, the embryo heads were dissected in phosphate buffered saline (PBS), fixed in DMSO-methanol at -20 °C for one week and then processed in ascending grades of ethanol, cleared in xylene followed by paraffin impregnation and embedding. For immunostains, 4 µm thick microtome sections were deparaffined with descending grades of ethanol. The sections were treated with 0.4% Triton X 100 (Sigma-Aldrich, Saint Louis, MA, USA) in PBS for 30 min and blocked using 10% normal goat serum (NGS) or Mouse IgG (Vector Laboratories, CA, USA). The sections were incubated with primary antibodies in suitable predetermined dilutions overnight, rinsed in PBS-Tween20 and incubated with corresponding Alexa 568 or 488 (Molecular Probes, Invitrogen, Eugene, OR, USA) conjugated secondary antibodies in dark for 2 h at room temperature. The immunostained sections were mounted in Vectashield (Vector laboratories, Burlingame, CA, USA) containing DAPI. The following primary antibodies were used: PAX-6 (1:400; cat# AB2237, Millipore, Princeton, MA, USA), Tuj-1 (1:500; cat# MMS435P, Covance, Burlington, NJ, USA), nestin (1:500; cat# MAB353, Millipore, Princeton, MA, USA) and phosphohistone-3 (p-H3, Cat# 06-570, 1:300 Millipore, Princeton, MA, USA). Alternatively, the embryo heads were fixed in 4% paraformaldehyde (PFA) for 24 h, cryoprotected in 10% and 20% sucrose for 24 h and finally frozen in liquid nitrogen, cut in 20 µm thick cryosections and stained as described above.

1  
2  
3  
4  
5  
6  
7  
8  
9  
10  
11  
12  
13  
14  
15  
16  
17  
18  
19  
20  
21  
22  
23  
24  
25  
26  
27  
28  
29  
30  
31  
32  
33  
34  
35  
36  
37  
38  
39  
40  
41  
42  
43  
44  
45  
46  
47  
48  
49  
50  
51  
52  
53  
54  
55  
56  
57  
58  
59  
60

Calbindin staining was performed using TSA amplification kit (Perkin Elmer, Waltham, MA, USA) according to the manufacturer instructions. Briefly, the deparaffinized sections were treated in 0.3% H<sub>2</sub>O<sub>2</sub> in methanol to quench endogenous peroxidase activity, blocked and incubated with primary antibody Calbindin D28K (1:500; cat# D28K Ab 1778, Millipore, Princeton, MA, USA) overnight. After washing the sections were incubated with biotinylated secondary antibody Vector BA 1000, (1:500, Vector Laboratories, Burlingame, CA, USA) followed by incubation with streptavidin-horseradish peroxidase conjugate. After amplification with fluorophore tyramide (1:300 dilution) the sections were washed, the nuclei stained with Hoechst (Sigma-Aldrich, Louis, MO, USA) and slides were mounted in mounting medium (Vecta Laboratories, Burlingame, CA, USA).

Immunohistochemical analysis was carried out blinded to the study groups in three anatomically matched sections from the rostrocaudal axis of *Cln5*<sup>-/-</sup> and WT embryos. Different layers in the dorsal telencephalon were identified according to Bayer and Altman (45) on the basis of cell morphology and density at 20x magnification. VZ was identified as a cellular region adjacent to ventricles having parallel arrays of cells with elongated nuclei perpendicular to the ventricle. The SVZ consists of disorganized compact layer of cells with rounded nuclei. In the current study, we did not differentiate VZ/SVZ, but pooled them in the analysis of progenitor population zones. The IZ was identified as a cell layer that was less dense than the proliferative VZ/SVZ, with the cells having a tangential orientation. The sub plate (SP) was recognized as a less dense layer below CP with large rounded nuclei. The CP layer had a higher cell density than IZ, with cells having a palisade like arrangement. Mid-dorsal telencephalon of the embryo brain sections was visualized at 10x magnification with Leica AX70 microscope, and immunoreactivity per unit area in the



different layers identified using the above defined criteria was quantified using 200-400  $\mu\text{m}$  wide window with Image Pro Plus 6.0 software. After the analysis, representative images of the E14.5 stainings were imported into Photoshop CC 2015 and pseudocolored by converting to gray scale and RGB, and then applying gradient maps with similar parameters to all images. Quantified results were expressed as mean  $\pm$  standard deviation (SD).

### **Cresyl violet staining**

The paraffin-processed sections were deparaffinized and stained in 0.1% cresyl violet acetate (Sigma Aldrich, St. Louis, MO, USA) for 5 min. After rinsing in tap water, the stained sections were differentiated in a solution of 96% ethanol with a few drops of acetic acid. Thereafter, the sections were dehydrated with ascending grades of 70% and absolute alcohol, cleared in xylene and finally mounted in DePeX (BDH, UK). The radial thickness of the dorsal telencephalon was quantified from three different locations along the length of the dorsal telencephalon and mean obtained from both sides of the brain. At least three anatomically matching embryonic sections along the rostrocaudal axis were analyzed in both WT and *Cln5*<sup>-/-</sup> mice.

### **Parvalbumin staining**

Parvalbumin staining was performed on 6-month-old WT and *Cln5*<sup>-/-</sup> mouse brain sections by Ni-DAB (Nickel-Diaminobezidine) method. Briefly the paraformaldehyde (PFA)-fixed 20 $\mu\text{m}$  cryo-sections from adult mice were washed in phosphate buffered saline (PBS). The antigen retrieval was performed by boiling sections in 0.05 M citrate buffer at 84°C for 30 min. Next, the blocking of endogenous peroxidase was performed by treating the sections with 0.3% H<sub>2</sub>O<sub>2</sub> in methanol for 30 min followed by washing in PBS with tween (PBST). The sections were treated with anti-

parvalbumin primary antibody (1:750, cat# 235 Swant, Switzerland) with an overnight incubation in a humidified chamber. The following day the sections were washed with PBST and treated with biotin conjugated secondary antibody (Vector Laboratories, Burlingame, CA, USA) at 1:200 dilution followed by treatment with ABC reagent (Vector Laboratories, Burlingame, CA, USA) for 30 min. For color development, the sections were treated with Ni-DAB solution supplemented with 0.075% H<sub>2</sub>O<sub>2</sub>. Color development was checked under the microscope and the reaction was stopped by immersion in double-distilled water. All test and control slides were treated similarly. This was followed by dehydration in ascending grades of alcohol, clearing in xylene and mounting in DePeX (BDH, UK).

**TUNEL assay**

Terminal deoxynucleotidyl transferase dUTP nick end labeling (TUNEL) staining was performed according to manufacturer instructions (Roche Diagnostics, Mannheim, Germany). Briefly, 20 µm thick 4% PFA fixed E14.5 embryo brain sections were air-dried and rehydrated in PBS. Antigen retrieval was performed in 0.05M citrate buffer at 80°C for 30 min or in a microwave oven at 750W for 1 min followed by rapid cooling. TUNEL reaction mixture was added to the test slides followed by incubation in a humidified chamber at 37°C for 1 h. The positive control was treated with DNAase I (Sigma Aldrich, St. Louis, MO, USA), and for the negative control slides the enzyme solution was omitted from the treatment. TUNEL positive cells were counted through the entire telencephalic wall from the ventricle to the pial surface from both hemispheres of the embryonic brain, and a mean count obtained from 2-3 anatomically matching sections along the rostrocaudal axis for both WT and *Cln5*<sup>-/-</sup> mice blinded to the study groups.

## 488 RNA isolation and semi-quantitative PCR

489 REST gene expression was analyzed by semi-quantitative PCR (qPCR) in mouse primary neurons,  
490 mouse primary microglia, neuronal progenitor cells, and mouse E14.5 and E17.5 cortical samples.  
491 Ptf1a gene expression was analyzed for in mouse E14.5 samples, and E17.5 cortical samples and  
492 NS5 cells. RNA was isolated from cortical samples dissected from E14.5 embryos using Trizol  
493 reagent according to the manufacturer's instructions. The concentration and purity was measured  
494 using NanoDrop 100 spectrophotometer (Thermo Fisher Scientific, Waltham, MA, USA). For  
495 cDNA synthesis, 500 ng of RNA was reverse transcribed (Thermo Fisher Scientific) according to  
496 the manufacturer's instructions. qPCR was performed using AB applied Biosystems StepOnePlus  
497 Real-Time PCR System® running StepOne Software® v 2.2.2. In all the experiments, all samples  
498 were run in duplicates and normalized to GAPDH housekeeping gene control and presented as  
499 fold change in the expression using the  $2^{-\Delta\Delta C_t}$  method where  $C_t$  is the threshold-cycle value.

500

## 501 Western blotting

502 Western blot for REST was performed on E14.5 cortical tissue samples isolated from *Cln5<sup>-/-</sup>* and  
503 WT embryos. Equal amounts of protein were loaded onto 10% SDS-PAGE gels and separated  
504 using a Mini-Protean 3 (Bio-Rad) device with 200 V. The separated proteins were transferred onto  
505 Hybond-P membrane (GE Healthcare) and blocked using 5% skimmed milk in PBS with 1%  
506 Tween20. The primary anti-REST antibody (1:1000 dilution, Cat# NRSF (P-18) sc-15118, Santa  
507 Cruz Biotechnology, Dallas, Texas, USA) was incubated overnight at 4°C, and after secondary  
508 HRP-labelled antibody incubation (1:2000 dilution, GE Healthcare) the immunoreactivities were  
509 developed using Pierce ECL Plus substrate (Thermo Fischer). Anti- $\beta$ -actin was used as a loading  
510 control and anti-mouse Cy5 as a secondary antibody (1:1000, Cat# 715-175-151, Jackson

1  
2  
3  
4  
5  
6  
7  
8  
9  
10  
11  
12  
13  
14  
15  
16  
17  
18  
19  
20  
21  
22  
23  
24  
25  
26  
27  
28  
29  
30  
31  
32  
33  
34  
35  
36  
37  
38  
39  
40  
41  
42  
43  
44  
45  
46  
47  
48  
49  
50  
51  
52  
53  
54  
55  
56  
57  
58  
59  
60

ImmunoResearch). The immunoreactivities were visualized on Storm 860 Fluoroimages (GE Healthcare) and intensities quantified using ImageQuant software (GE Healthcare).

**Neurite Outgrowth**

The neurite outgrowth dynamics were studied using IncuCyte ZOOM™ (Essen BioScience, Ann Arbor, MI, USA) live content imaging platform. Briefly, primary cortical neuronal cultures derived from E16 *Cln5*<sup>-/-</sup> and WT embryos were prepared as described by Byts *et al.* (46). Cells were seeded in 96-well plates at a density of 30000/cm<sup>2</sup> and cultured in MEM/B27 medium (Invitrogen, Carlsbad, CA, USA) supplemented with sodium bicarbonate, sodium pyruvate, L-glutamine, penicillin, streptomycin and 0.6% glucose. Cultures were incubated at 37°C under 5% CO<sub>2</sub>/95% air and 90% humidity without medium exchange up to six days. Images were taken each 24 h by IncuCyte ZOOM™. Finally, images were analyzed by Neuro Track™ software (Essen BioScience, Ann Arbor, MI, USA) to produce data on neurite dynamics during an extended period of growth. In each experiment, ~3000 neurons from 36 non-overlapping images from twelve wells were analyzed per condition.

**Tangential migration analysis**

Interneurons migrate from the GEs of the ventral telencephalon towards the dorsal telencephalon, by tangential migration. This interneuron migration was assessed by placing a window measuring about 200 μm in width spanning the entire telencephalic wall at the confluence of dorsal telencephalon and ventral telencephalon. Calbindin immunoreactive cells in this window that

represented the migrating interneurons were quantified in both WT and *Cln5<sup>-/-</sup>* embryos with Image Pro-Plus or Image J to estimate the flux of cellular migration as described earlier (47).

### **NS5 cell culture and treatment**

The mouse neural stem cell line NS5 cells were a kind gift from Prof. Austin Smith, University of Edinburgh, UK and cultured as described (22) in NS-A media (Euroclone S.p.A, Pero, Italy) with 10 ng/ml bFGF, 10 ng/ml EGF (both Peprotech, London, UK), 50.25 µg/ml pathocyte, 100 µg/ml apotransferrin, 16 µg/ml putrescine dihydrochloride, 25 µg/ml insulin, 19.8 ng/ml progesterone, 0.03 µM sodium selenite, 1.9 mM L-glutamine (all from Sigma). Cells were infected with an adenovirus expressing green fluorescent protein (GFP) or an adenovirus expressing GFP and the DNA-binding domain of REST (DN:REST) for 48 h at which point cells were approximately 80% confluent and 70% expressing the adenovirus as judged by GFP fluorescence. NS5 were infected with recombinant adenoviruses: (Ad-) control empty adenovirus, or (Ad DN:REST) dominant-negative construct (36). Purified adenovirus was added to subconfluent cells at the minimum titer, such that > 90% of cells became GFP-fluorescent with minimal cell death. RNA was harvested 48 h post-infection. The efficacy of DN:REST overexpression in depressing target gene expression and of siRNAs in knocking down REST mRNA has been validated by Bibel et al. (48).

### **Identification of REST target genes in NS5 cells by microarray analysis**

We utilised a database of RE1 elements in the mouse genome to create a microarray consisting of 574 RE1 elements found across the mouse genome and allow genome wide identification of REST occupancy in NS5 NSCs. In addition, features representing 40 control regions not in the vicinity of an RE1 element were included and used as the background. Input DNA and ChIP DNA were



1  
2  
3  
4  
5  
6  
7  
8  
9  
10  
11  
12  
13  
14  
15  
16  
17  
18  
19  
20  
21  
22  
23  
24  
25  
26  
27  
28  
29  
30  
31  
32  
33  
34  
35  
36  
37  
38  
39  
40  
41  
42  
43  
44  
45  
46  
47  
48  
49  
50  
51  
52  
53  
54  
55  
56  
57  
58  
59  
60

labelled with two different cyanine dyes (Cy3 and Cy5) and used to interrogate the array. The ratio of ChIP DNA: input DNA could then be calculated and normalised to the ratio for the control regions. The control regions were not occupied by REST and showed a 1:1 ratio ChIP DNA: input DNA. Similarly, putative RE1s that showed a 1:1 ratio were deemed unoccupied by REST. Of the RE1 sites on the array, RE1 elements associated with 151 genes were found to have an enrichment ratio above the input of 2 fold or more, from an average of three biological repeats (independent experiments). The control regions used on the array were found to provide a range of signal intensities in the input channel with an average of  $1.24 \pm 0.18$ . Data are shown in SI appendix Table S1 for all RE1 bindings sites showing enrichment >2-fold.

**Reverse transcription PCR**

Reverse transcription (RT) PCR was performed as described previously by Ooi et al. (49). Briefly, the cells were harvested in 1 ml Tri-reagent (Sigma), RNA-purified as per the manufacturer's instructions, and resuspended in 50 µl of Tris-EDTA, pH 8.0. Genomic DNA was removed by incubation with 1 µl of DNase (2 units) and 5 µl of 10× buffer (Ambion) for 30 min at 37 °C. 5 µg of RNA was made up to 50 µl with Milli-Q water and was reverse-transcribed with 2.5 µl of random primers (1.25 µg) and 2.5 µl of oligo(dT) (1.25 µg), 20 µl of 5× buffer, 20 µl of 8 mM dNTPs, 2.5 µl of RNasin (100 units), and 2.5 µl of Moloney murine leukemia virus H(–) reverse transcriptase (500 units) at 37 °C for 60 min. cDNA samples were purified using a PCR purification kit (Qiagen), and of the resulting 100 µl cDNA, 2 µl was used in a 20-µl real-time PCR reaction in duplicates in a Bio-Rad iCycler MyiQ. Non-reverse-transcribed RNA samples were included in the PCR to control for genomic DNA contamination.

1  
2  
3 578 The Ptf1a gene expression primer sequences were:  
4  
5  
6 579

7  
8 580 Sense – CTTGCAGGGCACTCTCTTTC  
9

10 581 Anti-sense – AGTTTTCTGGGGTCCTCTGG  
11  
12 582

13  
14  
15 583 **Chromatin Immunoprecipitation**  
16

17 584 The chromatin immunoprecipitation was carried out as described by Ooi et al. (49). Briefly, after  
18  
19 585 washing the cells with PBS, the cells were cross-linked with 1% formaldehyde for 10 min at room  
20  
21 586 temperature. After quenching with glycine, the cells were harvested and the chromatin was  
22  
23 587 fragmented into ~500-bp lengths by sonication. The chromatin was precleared with 5% bovine  
24  
25 588 serum albumin-blocked protein G-Sepharose and incubated with primary antibodies or control  
26  
27 589 IgG. After incubating the chromatin-antibody complexes with protein G-Sepharose beads, the  
28  
29 590 chromatin-antibody-bead complexes were collected by centrifugation, washed and eluted with 1%  
30  
31 591 SDS in 100 mM NaHCO<sub>3</sub>. The samples were de-cross-linked by incubation at 65 °C for 6 h, and  
32  
33 592 treated with 0.5 µl of 10 mg/ml RNase and 9 µl of 25 mg/ml proteinase K. Thereafter the DNA  
34  
35 593 was purified by phenol-chloroform extraction and resuspended in 100 µl water. Anti-REST  
36  
37 594 antibody (Cat# NRSF (H-290) sc-25398X) from Santa Cruz Biotechnology was used. PCR primers  
38  
39 595 were designed proximal to RE1s, and qPCR was performed in duplicates. The fold enrichment  
40  
41 596 was calculated by dividing the starting quantities of DNA in the immunoprecipitated samples by  
42  
43 597 that of the control antibody (IgG for affinity-purified antibodies or normal rabbit serum for crude  
44  
45 598 sera antibody preparations).  
46  
47  
48  
49  
50

51 599

52  
53  
54 600 The Ptf1a RE1 primers were:  
55  
56  
57  
58  
59  
60

1  
2  
3  
4  
5  
6  
7  
8  
9  
10  
11  
12  
13  
14  
15  
16  
17  
18  
19  
20  
21  
22  
23  
24  
25  
26  
27  
28  
29  
30  
31  
32  
33  
34  
35  
36  
37  
38  
39  
40  
41  
42  
43  
44  
45  
46  
47  
48  
49  
50  
51  
52  
53  
54  
55  
56  
57  
58  
59  
60

601 Sense – CAGGAGCCTTCCCTTTTCTT

602 Antisense - AAGCGCGTTTCGTAGATTGT

603

604 The *Gad1* RE1 primers were:

605 Sense - GCTCAGCGGGATATTGAAAA

606 Antisense - CTTTGACGCAAAACTCGATG

607

608 For the tissue samples chromatin immunoprecipitation was performed as previously by  
609 Mascanfroni et al. (50) with few modifications. Briefly, hippocampal tissue samples from 5  
610 months old mice were dissected out and homogenized over ice in PBS with Ultra-Turrax  
611 homogenizer (Daigger Scientific Inc, Vernon Hills, IL, USA), cross-linked with 1%  
612 paraformaldehyde and quenched with glycine after which the samples were washed twice with  
613 PBS and lysed with cell lysis buffer (50 mM Tris-HCl, pH 7.6, 1mM CaCl, 0.2% Triton, 5mM  
614 sodium butyrate and 50 µg/ml PMSF) over ice for 15 min. The chromatin pellet was collected with  
615 centrifugation and lysed with ChIP lysis buffer (10 mM Tris-HCl, pH 7.6, 10 mM EDTA, 0.1 %  
616 SDS, 10 mM Sodium butyrate and 50 µg/ml PMSF) and sonicated to shear the chromatin. 10 µg  
617 of antibody was prebound for 6 h to protein A– and protein G–Dynal magnetic beads (Invitrogen,  
618 USA), washed three times with ice-cold PBS plus 1% BSA, added to the chromatin diluted with  
619 ChIP incubation buffer (1% Triton X-100, 2 mM EDTA, 150 mM NaCl, 20 mM Tris-HCl, pH 8.0)  
620 and immunoprecipitated, with rotation, overnight. The magnetic bead–chromatin complexes were  
621 then washed three times with RIPA buffer (50 mM HEPES (pH 7.6), 1 mM EDTA, 0.7% Na  
622 deoxycholate, 1% NP-40, 0.5 M LiCl) followed by two times with TE buffer. Immunoprecipitated  
623 chromatin was then extracted with 1% SDS, 0.1 M NaHCO<sub>3</sub> and heated at 65 °C for 8 h to reverse

the paraformaldehyde cross-linking. DNA fragments were purified with a GeneJet Gel Extraction Kit (ThermoFisher Scientific, USA) and analyzed using the Taqman Fast Universal PCR Master Mix (#4367846, Life Technologies) and *gad1* (Mm04207432\_g1).

### EEG and power spectral density analysis

Two-month-old mice were implanted with an electrode assembly (WT male,  $n=6$ ; *Cln5*<sup>-/-</sup> male,  $n=7$ , WT female,  $n=7$ , *Cln5*<sup>-/-</sup> female,  $n=8$ ) under isoflurane anesthesia (induction: 4-4.5%, flow 400-450 ml/min; maintenance: 2-2.5 %, flow 200-220 ml/min). Briefly, the animal was secured into a stereotaxic frame (Kopf Instruments, Tujunga, CA, USA). A subcutaneous injection of lidocaine (0.3 ml, Lidocain 10 mg/ml, Orion, Espoo, Finland) was given under the scalp. Thereafter the scalp was opened with an incision and the skull was cleaned. Screw holes (electrodes and anchors) were drilled with a dental drill leaving the dura mater intact. The active electrodes were positioned bilaterally above the parietal cortex (anterior/posterior, AL: - 0.8 mm; medial/lateral, ML:  $\pm$  1.5 mm from bregma), and two screws on the frontal bone (AP: 1.5 mm; ML:  $\pm$  1.5 mm) served as the reference and ground electrodes. Three anchor screws were attached to the occipital and frontal bones. The screws were connected to a miniconnector (Mill-Max, Mouser Electronics, Mansfield, TX, USA) with insulated copper wire (diameter 200  $\mu$ m), and the whole construct was covered with dental acrylic cement. An i.p. injection of carprofen at 5 mg/kg was given to provide post-surgical analgesia (Rimadyl Vet 50 mg/ml, Zoetis, Helsinki, Finland). The animals were let to recover for 4 days after the surgery without handling. Thereafter, they were adapted to head-restraint for 3 consecutive days in 20-min daily sessions.

1  
2  
3  
4  
5  
6  
7  
8  
9  
10  
11  
12  
13  
14  
15  
16  
17  
18  
19  
20  
21  
22  
23  
24  
25  
26  
27  
28  
29  
30  
31  
32  
33  
34  
35  
36  
37  
38  
39  
40  
41  
42  
43  
44  
45  
46  
47  
48  
49  
50  
51  
52  
53  
54  
55  
56  
57  
58  
59  
60

The EEG signal from the parietal screw was referred to a frontal screw and recorded in calm head-fixed mice for 5 min. The signal was amplified (1000 x) with an AC amplifier (A-M Systems Inc., Sequim, WA, USA), bandpass-filtered between 1-1000 Hz and digitized at 2 kHz. The data were acquired by SciWorks 7.2 program (DataWave Technologies, Loveland, CO, USA). The power spectral density (PSD) was estimated using Welch’s method of spectral estimation using MatLab (MatLab R2011, MathWorks, Natick, MA, USA). PSD was inspected between 4-46 Hz in 1 Hz bins. The bins were grouped as frequency bands of 4-10 Hz (theta), 11-16 Hz (alpha), 17-30 Hz (beta) and 31-46 Hz (gamma), and the PSDs at each bin within these frequency bands were averaged for analysis. The EEG was recorded at 2 months and at 6 months of age. All recordings were carried out blinded to the study groups.

**Auditory-evoked potentials**

Auditory-evoked potentials (AEPs) were recorded after acquisition of EEG signal for the PSD analysis using the auditory gating paradigm. Mice remained head-fixed and the AEPs were evoked using a pair of click tones (conditioning and test tones, 500 ms between a pair of clicks, inter-stimulus interval 10 s; both tones: 3 kHz, duration 10 ms, 70 dB). A total of 30 click-pairs were delivered and responses were averaged for analysis. In the offline analysis, a baseline was determined as the average amplitude at -100 to 0 ms from the stimulus onset, for each AEP response. The first major negative deflection at around 40 ms from the stimulus onset was defined as N1, and its amplitude was measured from the baseline to the peak. Only the N1 component was included in the statistical analysis due to high variability in late occurring AEP components. Recordings that did not present typical AEP waveform (*i.e.* major negative deflection at ~40 ms and positive 100-200 ms from stimulus onset) were removed from analysis. Paired-pulse inhibition



669 was assessed by dividing test tone amplitude by conditioning tone amplitude. All recordings were  
670 carried out blinded to the study groups.

671

## 672 **Rotarod**

673 Mice were tested with the accelerating Rota-Rod® apparatus (Ugo Basile, Comerio, Italy) for  
674 motor coordination and balance. The day before the test, the mice were accustomed to stay on  
675 constantly rotating (4 rpm) round rod (2 cm in diameter) in two consecutive 2-min sessions. On  
676 the test day, mice were first allowed to walk on the rod at constant speed (4 rpm) for 1 min. Then  
677 the timing was started and rod rotation accelerated from 4 rpm to 40 rpm steadily within 5 min.  
678 The time to fall off the rod (or turn three full rounds around with the rod) was recorded until a 6-  
679 min cut-off time. All mice were tested three times with a break of approximately one hour between  
680 trials. The mean fall-off time across the three trials was used in the analysis. Group sizes in rotarod  
681 are indicated in Supplementary Information (SI) appendix Table S2. Rotarod was carried out  
682 blinded to the study groups.

683

## 684 **Statistical analysis**

685 Statistical analysis was performed using GraphPad Prism 7 software (LaJolla, CA, USA).  
686 Student's T-test or nonparametric Mann-Whitney U-test were used to compare the  
687 immunohistochemical quantification results between *Cln5*<sup>-/-</sup> and WT samples (two-tailed tests).  
688 The electrophysiology and rotarod data analyses were performed using analysis of variance  
689 (ANOVA). Genotype-effects (between-subject factor), age-effects (within-subjects factor) and  
690 genotype-age interactions were tested. The ANOVAs were followed by Bonferroni's post-hoc  
691 tests. Results are displayed as mean ± SD and statistical significance was set at  $p < 0.05$ .

1  
2  
3  
4  
5  
6  
7  
8  
9  
10  
11  
12  
13  
14  
15  
16  
17  
18  
19  
20  
21  
22  
23  
24  
25  
26  
27  
28  
29  
30  
31  
32  
33  
34  
35  
36  
37  
38  
39  
40  
41  
42  
43  
44  
45  
46  
47  
48  
49  
50  
51  
52  
53  
54  
55  
56  
57  
58  
59  
60

692  
  
693  
  
694  
  
695  
  
696  
  
697  
  
698  
  
699  
  
700  
  
701  
  
702  
  
703  
  
704  
  
705  
  
706  
  
707  
  
708  
  
709  
  
710  
  
711  
  
712

**Acknowledgements**

This study was supported by the Academy of Finland. H.L. was supported by Doctoral Program of Molecular Medicine at the University of Eastern Finland, and by Predoctoral Research Grants from Eye and Tissue Bank Foundation (Finland), The Finnish Cultural Foundation and Kuopio University Foundation, and by Postdoctoral Research Grants from Fight for Sight (USA), Eye and Tissue Bank Foundation, The Osk. Huttunen Foundation, The Finnish Cultural Foundation and Orion Research Foundation. We thank Ms. Mirka Tikkanen, Stefano Doccini and Filippo Santorelli for technical assistance.

**Conflict of Interest Statement:**

The authors have no conflict of interest to declare.

## References

- 1 Haltia, M. (2006) The neuronal ceroid-lipofuscinoses: from past to present. *Biochim. Biophys. Acta*, **1762**, 850-856.
- 2 Rider, J.A. and Rider, D.L. (1988) Batten disease: past, present, and future. *Am. J. Med. Genet. Suppl.*, **5**, 21-26.
- 3 Santavuori, P. (1988) Neuronal ceroid-lipofuscinoses in childhood. *Brain Dev.*, **10**, 80-83.
- 4 Goebel, H.H. (1996) The neuronal ceroid-lipofuscinoses. *Semin. Pediatr. Neurol.*, **3**, 270-278.
- 5 Josephson, S.A., Schmidt, R.E., Millsap, P., McManus, D.Q. and Morris, J.C. (2001) Autosomal dominant Kufs' disease: a cause of early onset dementia. *J. Neurol. Sci.*, **188**, 51-60.
- 6 Williams, R.E. and Mole, S.E. (2012) New nomenclature and classification scheme for the neuronal ceroid lipofuscinoses. *Neurology*, **79**, 183-191.
- 7 Wisniewski, K.E., Kida, E., Connell, F. and Zhong, N. (2000) Neuronal ceroid lipofuscinoses: research update. *Neurol. Sci.*, **21**, S49-56.
- 8 Uvebrant, P. and Hagberg, B. (1997) Neuronal ceroid lipofuscinoses in Scandinavia. Epidemiology and clinical pictures. *Neuropediatrics*, **28**, 6-8.
- 9 NCL Resource (2019). University College London, June 3th 2019, available at: <https://www.ucl.ac.uk/ncl-disease/mutation-and-patient-database/mutation-and-patient-datasheets-human-ncl-genes>
- 10 Holmberg, V., Jalanko, A., Isosomppi, J., Fabritius, A.L., Peltonen, L. and Kopra, O. (2004) The mouse ortholog of the neuronal ceroid lipofuscinosis CLN5 gene encodes a soluble lysosomal glycoprotein expressed in the developing brain. *Neurobiol. Dis.*, **16**, 29-40.

1  
2  
3 735 11 Isosomppi, J., Vesa, J., Jalanko, A. and Peltonen, L. (2002) Lysosomal localization of the  
4  
5 736 neuronal ceroid lipofuscinosis CLN5 protein. *Hum. Mol. Genet.*, **11**, 885-891.  
6  
7  
8 737 12 Tyynela, J., Suopanki, J., Santavuori, P., Baumann, M. and Haltia, M. (1997) Variant late  
9  
10 738 infantile neuronal ceroid-lipofuscinosis: pathology and biochemistry. *J. Neuropathol. Exp.*  
11  
12 739 *Neurol.*, **56**, 369-375.  
13  
14  
15 740 13 Kopra, O., Vesa, J., von Schantz, C., Manninen, T., Minye, H., Fabritius, A.L., Rapola, J.,  
16  
17 741 van Diggelen, O.P., Saarela, J., Jalanko, A. *et al.* (2004) A mouse model for Finnish variant late  
18  
19 742 infantile neuronal ceroid lipofuscinosis, CLN5, reveals neuropathology associated with early  
20  
21 743 aging. *Hum. Mol. Genet.*, **13**, 2893-2906.  
22  
23  
24 744 14 Heinonen, O., Kyttala, A., Lehmus, E., Paunio, T., Peltonen, L. and Jalanko, A. (2000)  
25  
26 745 Expression of palmitoyl protein thioesterase in neurons. *Mol. Genet. Metab.*, **69**, 123-129.  
27  
28  
29 746 15 Asada, H., Kawamura, Y., Maruyama, K., Kume, H., Ding, R.G., Kanbara, N., Kuzume,  
30  
31 747 H., Sanbo, M., Yagi, T. and Obata, K. (1997) Cleft palate and decreased brain gamma-  
32  
33 748 aminobutyric acid in mice lacking the 67-kDa isoform of glutamic acid decarboxylase. *Proc. Natl.*  
34  
35 749 *Acad. Sci. U S A*, **94**, 6496-6499.  
36  
37  
38 750 16 Lee, M.K., Tuttle, J.B., Rebhun, L.I., Cleveland, D.W. and Frankfurter, A. (1990) The  
39  
40 751 expression and posttranslational modification of a neuron-specific beta-tubulin isotype during  
41  
42 752 chick embryogenesis. *Cell Motil. Cytoskeleton*, **17**, 118-132.  
43  
44  
45 753 17 March, P.A., Wurzelmann, S. and Walkley, S.U. (1995) Morphological alterations in  
46  
47 754 neocortical and cerebellar GABAergic neurons in a canine model of juvenile Batten disease. *Am.*  
48  
49 755 *J. Med. Genet.*, **57**, 204-212.  
50  
51  
52 756 18 Braak, H. and Goebel, H.H. (1978) Loss of pigment-laden stellate cells: a severe alteration  
53  
54 757 of the isocortex in juvenile neuronal ceroid-lipofuscinosis. *Acta Neuropathol.*, **42**, 53-57.  
55  
56  
57  
58  
59  
60

- 1  
2  
3 758 19 Cooper, J.D., Messer, A., Feng, A.K., Chua-Couzens, J. and Mobley, W.C. (1999)  
4  
5 759 Apparent loss and hypertrophy of interneurons in a mouse model of neuronal ceroid lipofuscinosis:  
6  
7 760 evidence for partial response to insulin-like growth factor-1 treatment. *J. Neurosci.*, **19**, 2556-  
8  
9 761 2567.
- 11  
12 762 20 Savchenko, E., Singh, Y., Konttinen, H., Lejavova, K., Mediavilla Santos, L., Grubman,  
13  
14 763 A., Karkkainen, V., Keksa-Goldsteine, V., Naumenko, N., Tavi, P. *et al.* (2017) Loss of Cln5  
15  
16 764 causes altered neurogenesis in a mouse model of a childhood neurodegenerative disorder. *Dis.*  
17  
18 765 *Model Mech.*, **10**, 1089-1100.
- 20  
21 766 21 Gurevicius, K., Gureviciene, I., Valjakka, A., Schachner, M. and Tanila, H. (2004)  
22  
23 767 Enhanced cortical and hippocampal neuronal excitability in mice deficient in the extracellular  
24  
25 768 matrix glycoprotein tenascin-R. *Mol. Cell. Neurosci.*, **25**, 515-523.
- 27  
28 769 22 Ethridge, L.E., White, S.P., Mosconi, M.W., Wang, J., Byerly, M.J. and Sweeney, J.A.  
29  
30 770 (2016) Reduced habituation of auditory evoked potentials indicate cortical hyper-excitability in  
31  
32 771 Fragile X Syndrome. *Transl. Psychiatry.*, **6**, e787.
- 34  
35 772 23 Hershman, K.M., Freedman, R. and Bickford, P.C. (1995) GABAB antagonists diminish  
36  
37 773 the inhibitory gating of auditory response in the rat hippocampus. *Neurosci. Lett.*, **190**, 133-136.
- 39  
40 774 24 Schmiedt, M.L., Blom, T., Blom, T., Kopra, O., Wong, A., von Schantz-Fant, C., Ikonen,  
41  
42 775 E., Kuronen, M., Jauhiainen, M., Cooper, J.D. *et al.* (2012) Cln5-deficiency in mice leads to  
43  
44 776 microglial activation, defective myelination and changes in lipid metabolism. *Neurobiol. Dis.*, **46**,  
45  
46 777 19-29.
- 48  
49 778 25 Jones, B.J. and Roberts, D.J. (1968) A rotarod suitable for quantitative measurements of  
50  
51 779 motor incoordination in naive mice. *Naunyn Schmiedebergs Arch. Exp. Pathol. Pharmacol.*, **259**,  
52  
53 780 211.
- 55  
56  
57  
58  
59  
60

1  
2  
3  
4  
5  
6  
7  
8  
9  
10  
11  
12  
13  
14  
15  
16  
17  
18  
19  
20  
21  
22  
23  
24  
25  
26  
27  
28  
29  
30  
31  
32  
33  
34  
35  
36  
37  
38  
39  
40  
41  
42  
43  
44  
45  
46  
47  
48  
49  
50  
51  
52  
53  
54  
55  
56  
57  
58  
59  
60

781 26 Fabritius, A.L., Vesa, J., Minye, H.M., Nakano, I., Kornblum, H. and Peltonen, L. (2014)  
782 Neuronal ceroid lipofuscinosis genes, CLN2, CLN3 and CLN5 are spatially and temporally co-  
783 expressed in a developing mouse brain. *Exp. Mol. Pathol.*, **97**, 484-491.

784 27 Gotz, M., Stoykova, A. and Gruss, P. (1998) Pax6 controls radial glia differentiation in the  
785 cerebral cortex. *Neuron*, **21**, 1031-1044.

786 28 Bel-Vialar, S., Medevielle, F. and Pituello, F. (2007) The on/off of Pax6 controls the tempo  
787 of neuronal differentiation in the developing spinal cord. *Dev. Biol.*, **305**, 659-673.

788 29 von Schantz, C., Saharinen, J., Kopra, O., Cooper, J.D., Gentile, M., Hovatta, I., Peltonen,  
789 L. and Jalanko, A. (2008) Brain gene expression profiles of Cln1 and Cln5 deficient mice unravels  
790 common molecular pathways underlying neuronal degeneration in NCL diseases. *BMC Genomics*,  
791 **9**, 146.

792 30 von Schantz, C., Kielar, C., Hansen, S.N., Pontikis, C.C., Alexander, N.A., Kopra, O.,  
793 Jalanko, A. and Cooper, J.D. (2009) Progressive thalamocortical neuron loss in Cln5 deficient  
794 mice: Distinct effects in Finnish variant late infantile NCL. *Neurobiol. Dis.*, **34**, 308-319.

795 31 Lane, S.C., Jolly, R.D., Schmechel, D.E., Alroy, J. and Boustany, R.M. (1996) Apoptosis  
796 as the mechanism of neurodegeneration in Batten's disease. *J. Neurochem.*, **67**, 677-683.

797 32 Gupta, P., Soyombo, A.A., Atashband, A., Wisniewski, K.E., Shelton, J.M., Richardson,  
798 J.A., Hammer, R.E. and Hofmann, S.L. (2001) Disruption of PPT1 or PPT2 causes neuronal ceroid  
799 lipofuscinosis in knockout mice. *Proc. Natl. Acad. Sci. U S A*, **98**, 13566-13571.

800 33 Holopainen, J.M., Saarikoski, J., Kinnunen, P.K. and Jarvela, I. (2001) Elevated lysosomal  
801 pH in neuronal ceroid lipofuscinoses (NCLs). *Eur. J. Biochem.*, **268**, 5851-5856.



- 802 34 Haddad, S.E., Khoury, M., Daoud, M., Kantar, R., Harati, H., Mousallem, T., Alzate, O.,  
803 Meyer, B. and Boustany, R.M. (2012) CLN5 and CLN8 protein association with ceramide  
804 synthase: biochemical and proteomic approaches. *Electrophoresis*, **33**, 3798-3809.
- 805 35 Xu, Q., Cobos, I., De La Cruz, E., Rubenstein, J.L. and Anderson, S.A. (2004) Origins of  
806 cortical interneuron subtypes. *J. Neurosci.*, **24**, 2612-2622.
- 807 36 Tricoire, L., Pelkey, K.A., Erkkila, B.E., Jeffries, B.W., Yuan, X. and McBain, C.J. (2011)  
808 A blueprint for the spatiotemporal origins of mouse hippocampal interneuron diversity. *J.*  
809 *Neurosci.*, **31**, 10948-10970.
- 810 37 Mangan, S. and Alon, U. (2003) Structure and function of the feed-forward loop network  
811 motif. *Proc. Natl. Acad. Sci. U S A*, **100**, 11980-11985.
- 812 38 Abrajano, J.J., Qureshi, I.A., Gokhan, S., Zheng, D., Bergman, A. and Mehler, M.F. (2009)  
813 REST and CoREST modulate neuronal subtype specification, maturation and maintenance. *PLoS*  
814 *One*, **4**, e7936.
- 815 39 Moxon, K.A., Gerhardt, G.A., Bickford, P.C., Austin, K., Rose, G.M., Woodward, D.J.  
816 and Adler, L.E. (1999) Multiple single units and population responses during inhibitory gating of  
817 hippocampal auditory response in freely-moving rats. *Brain Res.*, **825**, 75-85.
- 818 40 Swaab, D.F., Chung, W.C., Kruijver, F.P., Hofman, M.A. and Hestiantoro, A. (2003) Sex  
819 differences in the hypothalamus in the different stages of human life. *Neurobiol. Aging*, **24 Suppl**  
820 **1**, S1-16; discussion S17-19.
- 821 41 Leinonen, H., Keksa-Goldsteine, V., Ragauskas, S., Kohlmann, P., Singh, Y., Savchenko,  
822 E., Puranen, J., Malm, T., Kalesnykas, G., Koistinaho, J. *et al.* (2017) Retinal Degeneration In A  
823 Mouse Model Of CLN5 Disease Is Associated With Compromised Autophagy. *Sci. Rep.*, **7**, 1597.

1  
2  
3  
4  
5  
6  
7  
8  
9  
10  
11  
12  
13  
14  
15  
16  
17  
18  
19  
20  
21  
22  
23  
24  
25  
26  
27  
28  
29  
30  
31  
32  
33  
34  
35  
36  
37  
38  
39  
40  
41  
42  
43  
44  
45  
46  
47  
48  
49  
50  
51  
52  
53  
54  
55  
56  
57  
58  
59  
60

824 42 Oswald, M.J., Palmer, D.N., Kay, G.W., Shemilt, S.J., Rezaie, P. and Cooper, J.D. (2005)  
825 Glial activation spreads from specific cerebral foci and precedes neurodegeneration in  
826 presymptomatic ovine neuronal ceroid lipofuscinosis (CLN6). *Neurobiol. Dis.*, **20**, 49-63.

827 43 Kay, G.W., Palmer, D.N., Rezaie, P. and Cooper, J.D. (2006) Activation of non-neuronal  
828 cells within the prenatal developing brain of sheep with neuronal ceroid lipofuscinosis. *Brain*  
829 *Pathol.*, **16**, 110-116.

830 44 Utriainen, A., Sormunen, R., Kettunen, M., Carvalhaes, L.S., Sajanti, E., Eklund, L.,  
831 Kauppinen, R., Kitten, G.T. and Pihlajaniemi, T. (2004) Structurally altered basement membranes  
832 and hydrocephalus in a type XVIII collagen deficient mouse line. *Hum. Mol. Genet.*, **13**, 2089-  
833 2099.

834 45 Bayer, S.A. and Altman, J. (1991) *Neocortical development*. Raven Press, New York.

835 46 Byts, N., Samoylenko, A., Fasshauer, T., Ivanisevic, M., Hennighausen, L., Ehrenreich, H.  
836 and Siren, A.L. (2008) Essential role for Stat5 in the neurotrophic but not in the neuroprotective  
837 effect of erythropoietin. *Cell Death Differ.*, **15**, 783-792.

838 47 Pozas, E. and Ibanez, C.F. (2005) GDNF and GFR $\alpha$ 1 promote differentiation and  
839 tangential migration of cortical GABAergic neurons. *Neuron*, **45**, 701-713.

840 48 Bibel, M., Richter, J., Schrenk, K., Tucker, K.L., Staiger, V., Korte, M., Goetz, M. and  
841 Barde, Y.A. (2004) Differentiation of mouse embryonic stem cells into a defined neuronal lineage.  
842 *Nat. Neurosci.*, **7**, 1003-1009.

843 49 Ooi, L., Belyaev, N.D., Miyake, K., Wood, I.C. and Buckley, N.J. (2006) BRG1 chromatin  
844 remodeling activity is required for efficient chromatin binding by repressor element 1-silencing  
845 transcription factor (REST) and facilitates REST-mediated repression. *J. Biol. Chem.*, **281**, 38974-  
846 38980.

847 50 Mascanfroni, I.D., Takenaka, M.C., Yeste, A., Patel, B., Wu, Y., Kenison, J.E., Siddiqui,  
848 S., Basso, A.S., Otterbein, L.E., Pardoll, D.M. *et al.* (2015) Metabolic control of type 1 regulatory  
849 T cell differentiation by AHR and HIF1- $\alpha$ . *Nat. Med.*, **21**, 638-646.

850

851

852

853

854

855

856

857

858

859

860

861

1  
2  
3  
4  
5  
6  
7  
8  
9  
10  
11  
12  
13  
14  
15  
16  
17  
18  
19  
20  
21  
22  
23  
24  
25  
26  
27  
28  
29  
30  
31  
32  
33  
34  
35  
36  
37  
38  
39  
40  
41  
42  
43  
44  
45  
46  
47  
48  
49  
50  
51  
52  
53  
54  
55  
56  
57  
58  
59  
60

**Figure legends**

**Figure 1. Cytoarchitectural changes at E14.5 in *Cln5*<sup>-/-</sup> embryos.** Nissl stained sections from E14.5 WT (**A, B, C**) and *Cln5*<sup>-/-</sup> embryos (**D, E, F**) show a significant reduction in the radial thickness of the dorsal telencephalon (DT) wall along the rostral (**G**) intermediate (**H**) and caudal (**I**) sections. Scale bar in A-F=100µm, magnification 4X, n=6 for WT, n=5 for *Cln5*<sup>-/-</sup>, \**P*<0.05, \*\**P*<0.01 with Student's T-test, data expressed as mean ± SD. The red horizontal bars in the pictures indicate radial thickness of the pallial wall. Representative images of Pax6 and Tuj1 immunoreactivity from WT (**J, L**) and *Cln5*<sup>-/-</sup> (**K,M**) embryonic DT. Scale bar 100µm, magnification 10X. The histograms in **N** and **O** show results from Pax6 and Tuj1 quantification from DT along the rostral caudal axis (rostral, intermediate and caudal dorsal telencephalon, respectively. \**P*<0.05, \*\**P*<0.01 with Student's T-test, data expressed as mean ± SD, n=6 or 7 for WT, n=5-6 for *Cln5*<sup>-/-</sup>.

**Figure 2. Loss of *Cln5* leads to increased apoptosis and proliferative deficits in the dorsal telencephalon (DT) at E14.5.** The TUNEL positive cells were visualized in the developing E14.5 (A) WT and (B) *Cln5*<sup>-/-</sup> brains. Scale bar 50µm, magnification 10X. The graph in C represents the quantification of TUNEL staining that was performed across the entire DT wall from the ventricles to the border of the pia, presented as average count from 2-3 sections along the rostral-caudal axis. \**P*<0.05 in Student's T-test, data expressed as mean ± SD, n=4 for WT, n=3 for *Cln5*<sup>-/-</sup>. The rate of proliferation in WT and *Cln5*<sup>-/-</sup> DT was examined by counting of p-H3 positive cells in rostral (D), intermediate (E) and caudal (F) DT. \**P*<0.05, with Student's T-test, data expressed as mean±SD, n=5-7 for both genotypes. CP = cortical plate, IZ = intermediate zone, SVZ = subventricular zone, VZ = ventricular zone.

1  
2  
3  
4  
5  
6  
7  
8  
9  
10  
11  
12  
13  
14  
15  
16  
17  
18  
19  
20  
21  
22  
23  
24  
25  
26  
27  
28  
29  
30  
31  
32  
33  
34  
35  
36  
37  
38  
39  
40  
41  
42  
43  
44  
45  
46  
47  
48  
49  
50  
51  
52  
53  
54  
55  
56  
57  
58  
59  
60

**Figure 3. Loss of *Cln5* affects interneuron populations and stem cell proliferation rate in the ganglionic eminences (GEs).** Calbindin, a marker for early interneurons, was assessed by immunostaining in the MGE in WT (**A**) and *Cln5*<sup>-/-</sup> embryos (**B**). Scale bar = 100μm, magnification 10X. The graphs in **C-D** show the quantification results of the calbindin immunoreactivity in MGE and LGE. \**P*<0.05 in Student's T-test, data expressed as mean ± SD, n=6-7 for WT, n=4-5 for *Cln5*<sup>-/-</sup>. The rate of proliferation in WT and *Cln5*<sup>-/-</sup> mice's GEs was examined by counting of p-H3 positive cells. Representative images show p-H3 staining in the MGE and LGE (**E-H**). E14.5 *Cln5*<sup>-/-</sup> embryos have a lower number of proliferating cells in the LGE and CGE in comparison to the WT embryos (**J-K**). Scale bar: 100μm, magnification: 10X. \**P*<0.05, *P*<0.01\*\* with Student's T-test, data expressed as mean ± SD. MGE = medial ganglionic eminence, LGE = lateral ganglionic eminence, CGE = caudal ganglionic eminence.



**Figure 4. Adult *Cln5*<sup>-/-</sup> mice exhibit alterations in Parvalbumin (PV) positive interneurons.**

Representative images from the hippocampi of 6-month-old WT (**A**) and *Cln5*<sup>-/-</sup> (**E**) mice show a reduced number of PV stained interneurons in the CA1 layer in *Cln5*<sup>-/-</sup> mice. Images **a1** and **b1** show an enlarged view of the area of the quantification in WT and *Cln5*<sup>-/-</sup> mice, respectively, and the graph **C** shows the quantification result. n=6 for WT, n=7 for *Cln5*<sup>-/-</sup>. The black arrows in **A** and **B** point to the boundary of 200µm distance where the quantification was performed. Images **D** and **E** show hilar PV interneurons from 6-month-old WT and *Cln5*<sup>-/-</sup> animals respectively. Quantification of the hilar region (**F**) revealed a significantly lower number of PV-positive interneurons in *Cln5*<sup>-/-</sup> mice compared to their WT controls. n=9 for WT, n=7 for *Cln5*<sup>-/-</sup>. The area surrounded by white dashed lines in **D** and **E** show the hilar region quantified for analysis while the white arrowheads point to the PV immunoreactive cells. The data was obtained from male and female mice. Scale bar for D-G is 50µm, magnification: 10X, \*\**P*<0.01, data expressed as mean ± SD.

**Figure 5. Loss of *Cln5* impairs neurite outgrowth.** Representative images of neurite outgrowth in WT (A) and *Cln5*<sup>-/-</sup> (B) cortical neurons. Scale bar: 80 μm, magnification: 10X. Dashed rectangles in A and B represent areas in magnified panels. Quantification of neurite length (C) was performed from two different embryos per genotype with more than 300 neurons analyzed per embryo. Quantification showed that the loss of *Cln5* decreases neurite length. \**P*<0.05 with one-way ANOVA, data expressed as mean ± SEM.

**Figure 6. REST levels are increased in adult *Cln5*<sup>-/-</sup> hippocampi and REST regulates genes involved in GABAergic neuron differentiation.** Representative image of the levels of REST protein in WT and *Cln5*<sup>-/-</sup> mouse hippocampi as assessed by Western blotting (A). Quantification of REST levels as normalized to  $\beta$ -actin revealed a significant increase in the levels of REST protein in *Cln5*<sup>-/-</sup> brains (B).  $n = 6-7$ ,  $*P < 0.05$ , data expressed as mean  $\pm$  SD. ChIP identified REST occupancy at known and novel RE1 sites. REST targets included genes involved in GABAergic neuron differentiation, including *Ptfla* and *Gad1* in NS5 cells (C). *Ptfla* expression is silenced by REST and inhibition of REST function de-represses *Ptfla* expression. *Ptfla* was silent in control adenovirus infected cells (control) and induced following infection of NS5 cells with dominant negative REST (DN:REST) (D). Expression is shown normalized to cyclophilin ( $\times 10^{-5}$ ). Data is shown as mean of three individual experiments each with minimum of three technical replicates. (E) Chip-qPCR assay from hippocampal samples of 5-month-old *Cln5*<sup>-/-</sup> mice show increased interaction of REST with *Gad1*.

1  
2  
3  
4  
5  
6  
7  
8  
9  
10  
11  
12  
13  
14  
15  
16  
17  
18  
19  
20  
21  
22  
23  
24  
25  
26  
27  
28  
29  
30  
31  
32  
33  
34  
35  
36  
37  
38  
39  
40  
41  
42  
43  
44  
45  
46  
47  
48  
49  
50  
51  
52  
53  
54  
55  
56  
57  
58  
59  
60

**Figure 7. Cortical hyperexcitability in adult *Cln5*<sup>-/-</sup> mice.** Auditory-evoked potentials (AEP) and power spectral density (PSD) analysis from EEG signal was used to investigate cortical hyperexcitability *in vivo*. The AEPs and EEG were collected in head-fixed awake mice (see Material & Methods for details). **A-D**: Group-averaged waveforms at 2 month of age for condition (**A,C**) and test (**B,D**) tones. (WT male, n=3; *Cln5*<sup>-/-</sup> male, n=5; WT female, n=6; *Cln5*<sup>-/-</sup> female, n=5). The condition and test tone (both tones: 3 kHz, 70 dB) was separated by 500 ms, and the tone-pair was delivered in 10 s intervals for 30 times. **E**: Condition tone amplitudes at 2 and 6 months of age. **F**: Test tone – condition tone ratio reveals impaired paired-pulse inhibition in *Cln5*<sup>-/-</sup> mice as compared to WT mice at 2-months of age (genders pooled, genotype effect:  $F_{1,35}=3.1$ ,  $P=0.09$ ; interaction:  $F_{1,35}=3.2$ ,  $P=0.08$ ). **G-J**: PSDs at 2 and 6 months of age. PSDs were analyzed from continuous (5 min) EEG recording (WT male, n=5(-6); *Cln5*<sup>-/-</sup> male, n=7; WT female, n=7; *Cln5*<sup>-/-</sup> female, n=8). PSDs at 1 Hz intervals were acquired and averaged for statistical analysis at theta (4-10 Hz), alpha (11-16 Hz), beta (17-30 Hz) and gamma (31-46 Hz) frequencies. Note the pronounced increase in PSD in male *Cln5*<sup>-/-</sup> mice but not in females, similarly as in response to condition tone in AEP experiment (**A** vs. **C**). Statistical analysis was performed by 2-way ANOVA followed by Bonferroni posthoc test: \* $P<0.05$ , \*\* $P<0.01$ . Data are presented as means  $\pm$  SD.

**Abbreviations:**

AEP, auditory evoked potential; CGE, caudal ganglionic eminences; CP, cortical plate; CNS, central nervous system; DT, dorsal telencephalon; EEG, electroencephalography; GEs, ganglionic eminences; IZ, intermediate zone; LGE, lateral ganglionic eminences; MGE, medial ganglionic eminences; NCL, neuronal ceroid lipofuscinosis; PSD, power spectral density; PV, parvalbumin; REST, repressor element 1-silencing transcription factor; SB, sub plate; SD, standard deviation; SVZ, subventricular zone; VZ, ventricular zone; WT, wild-type.

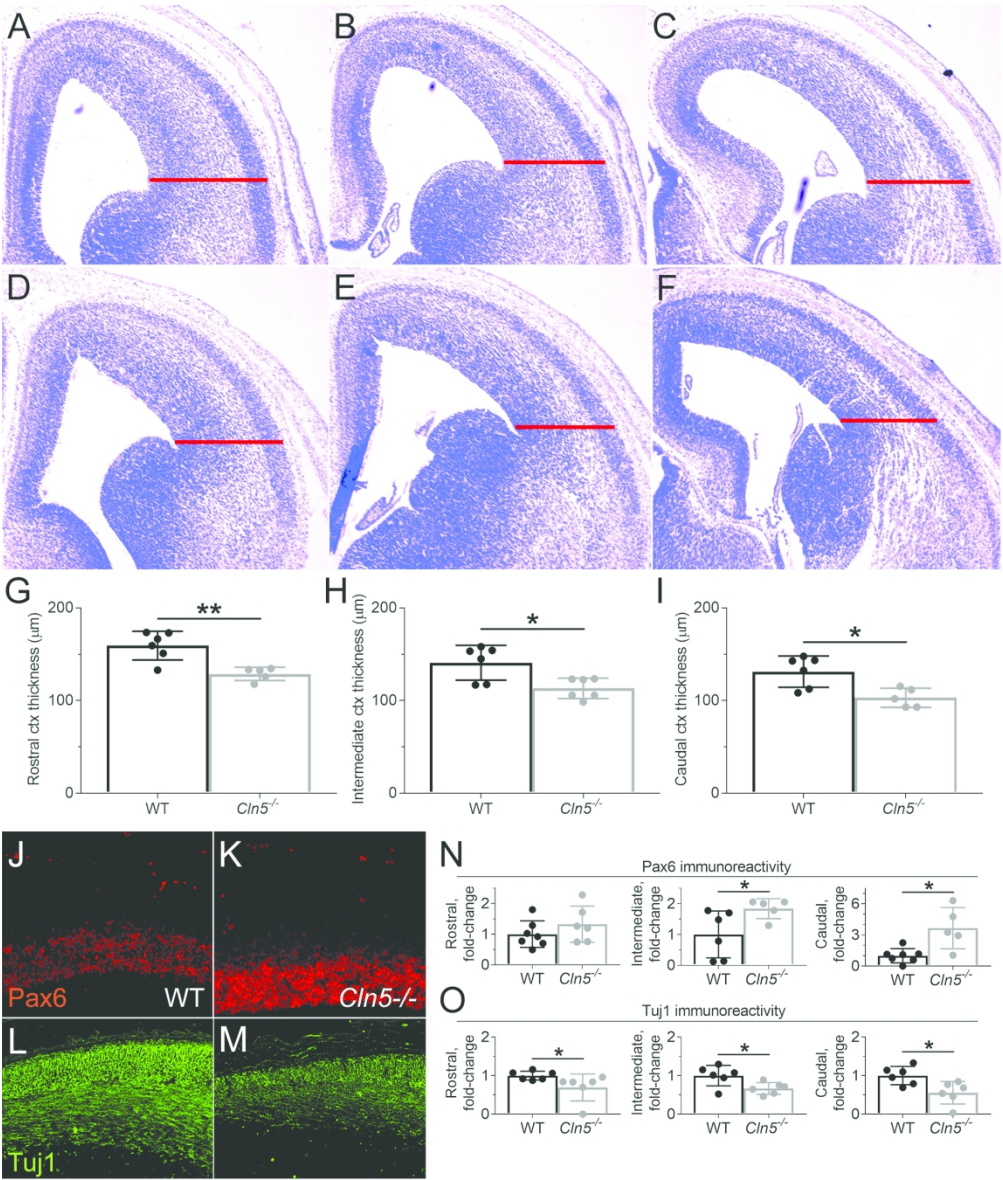


Figure 1. Cytoarchitectural changes at E14.5 in *Cln5*<sup>-/-</sup> embryos.



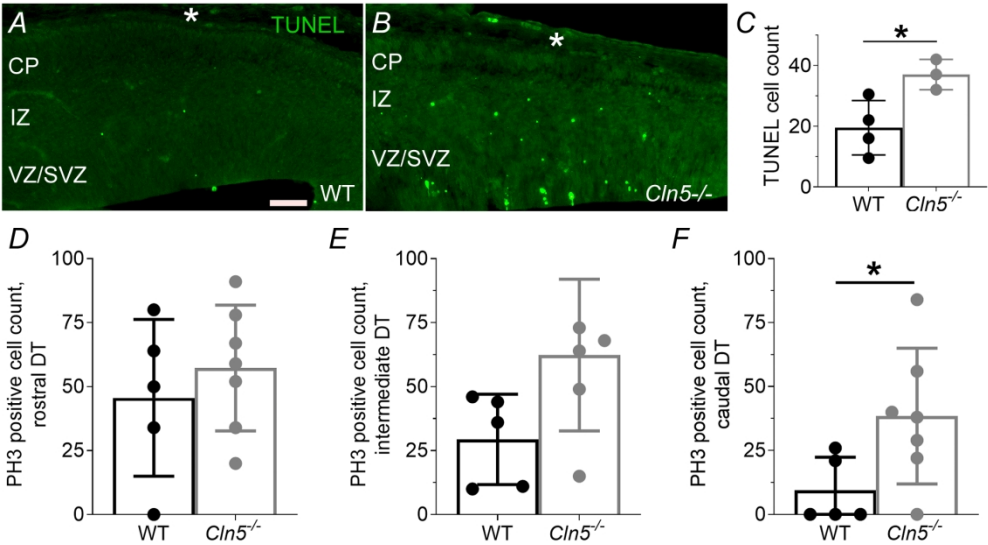
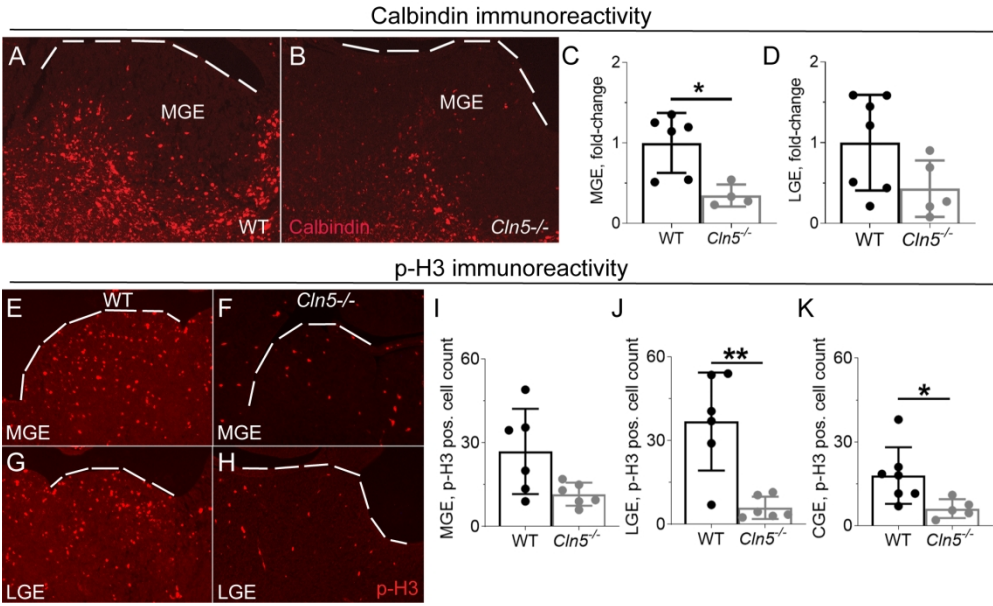


Figure 2. Loss of *Cln5* leads to increased apoptosis and proliferative deficits in the dorsal telencephalon (DT) at E14.5.



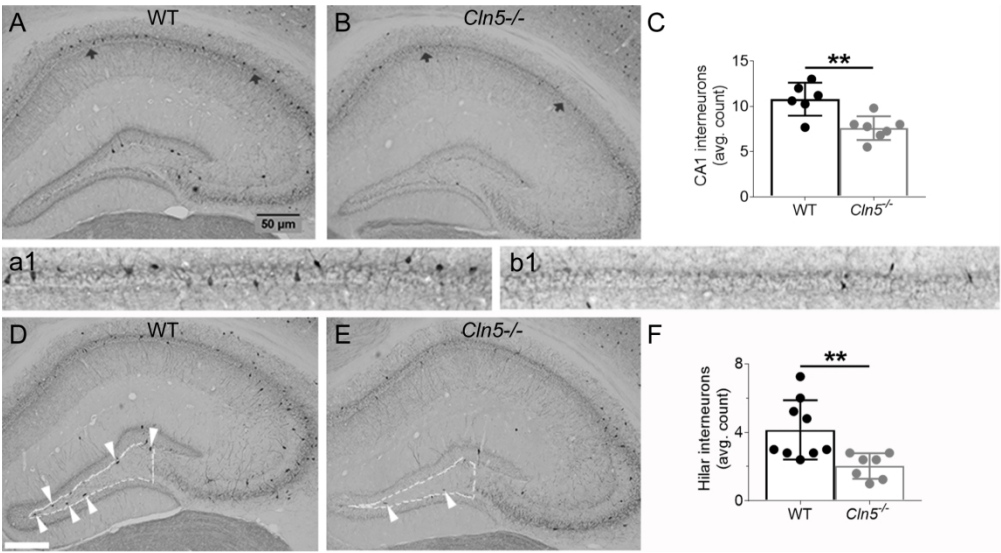


Figure 4. Adult Cln5<sup>-/-</sup> mice exhibit alterations in Parvalbumin (PV) positive interneurons.

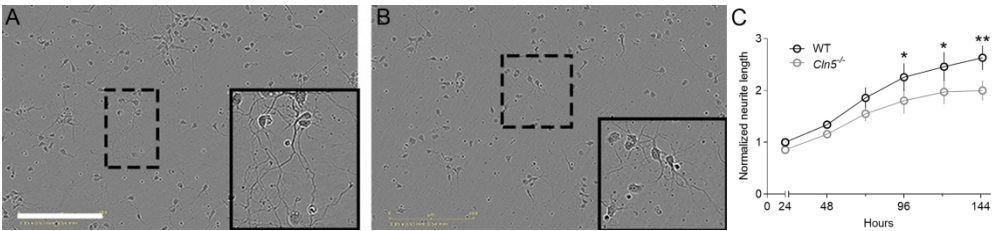


Figure 5. Loss of Cln5 impairs neurite outgrowth.

188x42mm (300 x 300 DPI)

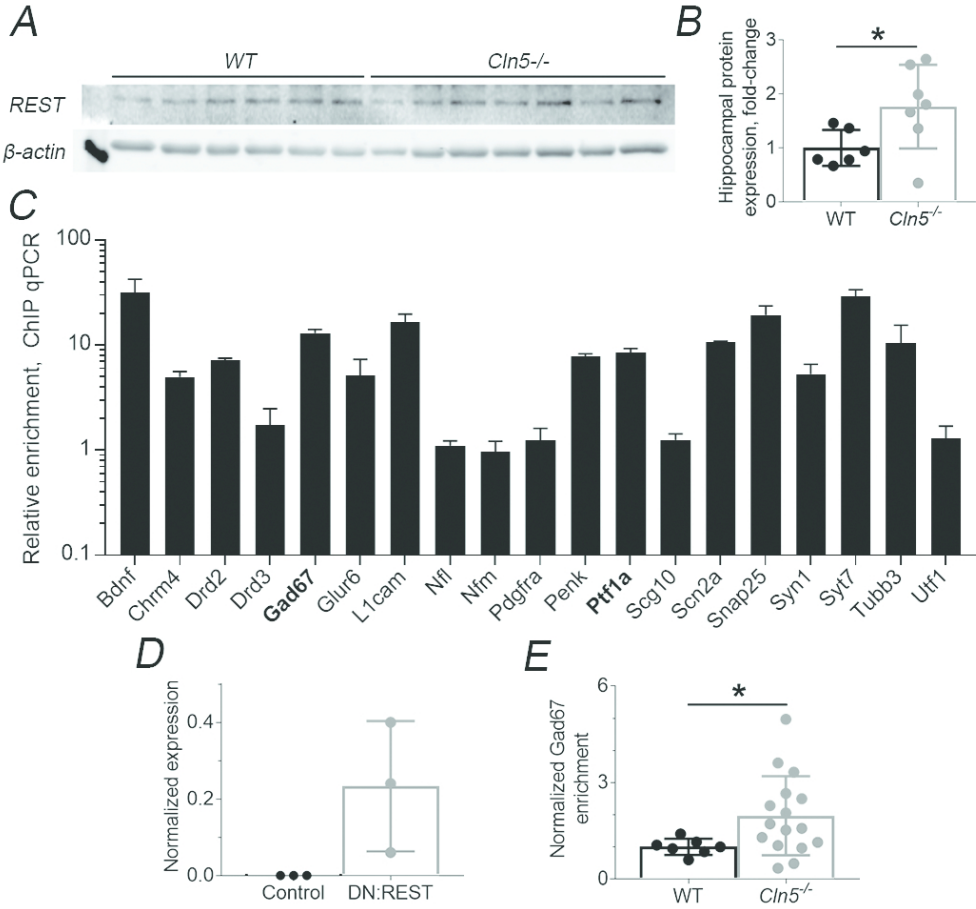


Figure 6. REST levels are increased in adult Cln5<sup>-/-</sup> hippocampi and REST regulates genes involved in GABAergic neuron differentiation.

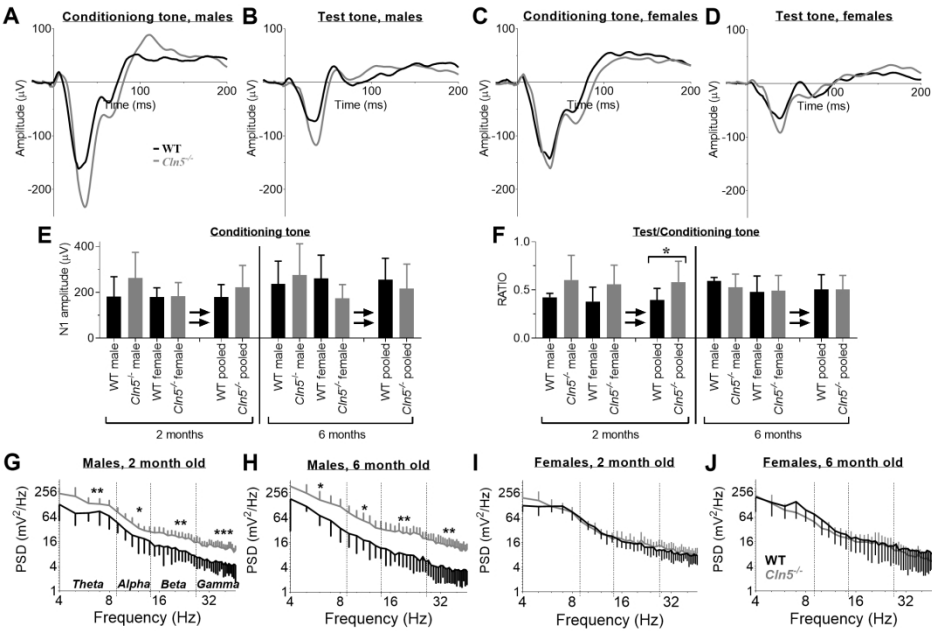


Figure 7. Cortical hyperexcitability in adult *Cln5*<sup>-/-</sup> mice.

200x131mm (300 x 300 DPI)